(12)

SECURITY CLASSIFICATION OF THIS PAGE (When Data Entered)

REPORT DOCUMENTATION PAGE

READ INSTRUCTIONS BEFORE COMPLETING FORM

1. REPORT NUMBER	2. GOVT ACCESSION NO. / 3. RECIPIENT'S CATALOG NUMBER
4. TITLE (and Subtitle): Application of Solidification Theory to Rapid Solidification Processing	5. TYPE OF REPORT & PERIOD COVERED: Semi-annual technical report April 1, 1983 to Sept. 30, 1983
	6. PERFORMING ORG. REPORT NUMBER
7. AUTHOR(s): W. J. Boettinger, J. W. Cahn, S. R. Coriell, J. R. Manning and R. J. Schaefer	8. CONTRACT OR GRANT NUMBER(s): ARPA Order 3751
9. PERFORMING ORGANIZATION NAME AND ADDRESS: Metallurgy Division, National Bureau of Standards, Gaithersburg, MD 20899	10. PROGRAM ELEMENT, PROJECT, TASK AREA & WORK UNIT NUMBERS: 4D10, 61101E
11. CONTROLLING OFFICE NAME AND ADDRESS: Materials Science Division, Defense Advanced Research Projects Agency, 1400 Wilson Boulevard, ...igton, VA 22209	12. REPORT DATE: July 1984
	13. NUMBER OF PAGES: 103
...ORING AGENCY NAME & ADDRESS (if different from Controlling Office)	15. SECURITY CLASS. (of this report)
	15a. DECLASSIFICATION/DOWNGRADING SCHEDULE

...IBUTION STATEMENT (of this Report)

...oved for public release. Distribution unlimited.

...BUTION STATEMENT (of the abstract entered in Block 20, if different from Report)

...PPLEMENTARY NOTES

19. KEY WORDS (Continue on reverse side if necessary and identify by block number)

Ag-Cu alloys; Alloy microstructure; Alloy phases; Extended solid solubility; NiAl-Cr quasibinary alloys; Rapid solidification; Solidification theory

20. ABSTRACT (Continue on reverse side if necessary and identify by block number)

Rapid solidification allows the production of alloys with new compositions and phases and also allows production of improved alloys by control of microstructures and homogeneity. The effect of rapid solidification velocity on the microstructure of Ag-Cu alloys is comprehensively described, mechanisms of microsegregation-free solidification are reviewed, and microstructure and phase solubility extension in rapidly solidified NiCr-Al quasibinary eutectic alloys are discussed in papers prepared for publication.

DD FORM 1 JAN 73 1473 EDITION OF 1 NOV 65 IS OBSOLETE

SECURITY CLASSIFICATION OF THIS PAGE (When Data Entered)

AD-A145 953

DTIC FILE COPY

DTIC ELECTE SEP 27 1984 S E

Application of Solidification Theory to Rapid Solidification Processing

W. J. Boettinger, J. W. Cahn, S. R. Coriell,
J. R. Manning, and R. J. Schaefer
Metallurgy Division
Center for Materials Science
National Bureau of Standards
Gaithersburg, MD 20899

Semi-Annual Technical Report
Period Covered: April 1, 1983 to September 30, 1983

Report Issued: July 1984

Prepared for
Defense Advanced Research Projects Agency
Arlington, Virginia 22209

Program Code No: 4D10
Effective Date of Contract: April 1, 1979
Contract Expiration Date: September 30, 1986
Principal Investigator: J. R. Manning (301/921/3354)

Table of Contents

Application of Solidification Theory to Rapid Solidification Processing

This semi-annual technical report for ARPA Order 3751 covers the period April 1, 1983 to September 30, 1983.

Task Objective

The objective of this work is to develop guidelines based on kinetic and thermodynamic solidification theory for prediction and control of rapid solidification processes. In particular, segregation effects and rules governing the formation of equilibrium and non-equilibrium phases, including metallic glasses, will be investigated. Areas where significant improvements in alloy properties can be produced by rapid solidification will be emphasized.

Technical Problem and General Methodology

Rapid solidification techniques make it possible to produce new types of materials having significantly better properties than conventionally processed materials. However, improved predictive techniques and control of rapid solidification processes are needed. The current studies are focussed on the science underlying areas where improved materials can be obtained in order to provide such prediction and control. This work is both theoretical and experimental.

Two major ways in which rapid solidification technology provides improved materials are:

1. Production of alloys with new compositions and phases.
2. Production of improved alloy properties by control of microstructures and homogeneity in rapidly solidified alloys.

The general method followed in this work has been to identify critical questions in these major rapid solidification application areas where solidification theory, when properly developed and checked by experiment, can provide improved understanding of important rapid solidification processes. This understanding then is pursued to provide guidelines that can be used by alloy producers to obtain new improved materials and to select optimum alloy compositions and processing conditions for rapid solidification applications.

Technical Results

1. Production of Alloys with New Compositions or Phases

Rapid solidification allows the partitionless solidification of alloys to produce extended solid solubility, i.e., production of single phase solidified alloys having compositions in two-phase regions of alloy phase diagrams. Production of uniform alloys in these composition ranges normally is not possible by conventional metal processing techniques. However, such homogeneous alloys would be expected to have properties not obtainable by other means. Furthermore, these alloys might be subsequently heat treated to provide very fine precipitates and, by that means, produce material with especially desirable properties. The conditions necessary for producing such alloys are being investigated in the present work to allow prediction and control of these processes.

Two papers which report details of our progress in this area are:

A. The Effect of Rapid Solidification Velocity on the Microstructure of Ag-Cu Alloys, W. J. Boettinger, D. Shechtman, R. J. Schaefer, and F. S. Biancaniello, Metallurgical Transactions 15A, 55-66 (January 1984).

B. Microstructure and Phase Solubility Extension in Rapidly Solidified NiAl-Cr Quasibinary Eutectic, D. Shechtman, W. J. Boettinger, T. Z. Kattamis, and F. S. Biancaniello, Acta Metallurgica 32, 749-756 (May 1984).

These papers are included in the appendix as part of this report. This work was done in collaboration with D. Shechtman, Johns Hopkins University, and T. Z. Kattamis, University of Connecticut, during times they spent at the National Bureau of Standards.

2. Production of Improved Alloy Properties by Control of Microstructures and Homogeneity in Rapidly Solidified Alloys

Even in cases where the equilibrium solid solubility is not exceeded, it is frequently possible to obtain striking improvements in alloy properties by means of rapid solidification. These improvements result from the differences in alloy microstructure and homogeneity resulting from rapid solidification. Conditions which will tend to produce homogeneous alloys either with or without accompanying extended solid solubility are being investigated.

A frequent microstructural feature of rapidly solidified alloys is the absence of cellular or dendritic microsegregation, often accompanied by incorporation of solute in excess of the equilibrium solid solubility. Two solidification mechanisms can produce microsegregation-free crystalline solids: planar growth and partitionless solidification. The solidification conditions required for planar growth with equilibrium partitioning at the interface are well known. For growth at high velocities, capillarity provides a stabilization of the planar interface. This regime is referred to as absolute stability and applies only when the net heat flow is toward the

solid. Partitionless solidification arises from the kinetics of interface motion. These kinetics can involve the trapping of solute by the moving interface, causing the partition coefficient to deviate from the equilibrium value. Solute trapping generally occurs at high interface velocities and may be pronounced when the interface temperature is far below the liquidus.

A paper that reports details of our studies on this topic is:

C. Mechanisms of Microsegregation-Free Solidification, W. J. Boettinger, S. R. Coriell, and R. F. Sekerka, Materials Science and Engineering, 65, 27-36 (1984).

This paper is included in the appendix as part of this report. This work was done in collaboration with R. F. Sekerka, Carnegie-Mellon University, during time he spent as a consultant at the National Bureau of Standards.

Published in Metallurgical Transactions 15A, 55-66 (January 1984).

The Effect of Rapid Solidification Velocity on the Microstructure of Ag-Cu Alloys

W. J. Boettinger, D. Shechtman, R. J. Schaefer, and F. S. Biancaniello

Electron beam solidification passes have been performed on a series of Ag-Cu alloys between 1 wt.% Cu and the eutectic composition (28.1 wt.% Cu) at speeds between 1.5 and 400 cm/s. At low growth rates conventional dendritic or eutectic structures are obtained. The maximum growth rate of eutectic structure is 2.5 cm/s. At high growth rates microsegregation-free single phase structures are obtained for all compositions. The velocity required to produce this structure increases with composition for dilute alloys and agrees with the theory of absolute stability of a planar liquid-solid interface with equilibrium partitioning. For alloys between 15 and 28 wt.% Cu, the velocity required to produce the microsegregation-free extended solid solution decreases with composition and is related to nonequilibrium trapping of solute at the liquid solid interface. At intermediate growth rates for alloys with 9 wt.% Cu or greater, a structure consisting of alternating bands of cellular and cell-free material is obtained. The bands form approximately parallel to the local interface.

W. J. Boettinger, R. J. Schaefer, and F. S. Biancaniello are in the Metallurgy Division, Center for Materials Science, National Bureau of Standards, Washington, DC 20234. D. S. Shechtman is in the Department of Materials Engineering, Technion, Haifa, Israel on leave at the Center for Materials Research, The Johns Hopkins University, Baltimore, MD 21218.

INTRODUCTION

Rapidly solidified crystalline alloys are well known to exhibit refined scales of microsegregation and interdendritic second phase particles. In some cases microsegregation and interdendritic phases can be completely eliminated by rapid solidification. These microsegregation-free structures can occur in alloys with compositions beyond the equilibrium solubility limit of the primary phase and provide an ideal starting microstructure for subsequent thermomechanical processing.

The splat-quenching experiments of Duwez, Klement, and Willens [1] showed by x-ray diffraction that complete solubility of Ag and Cu could be obtained in the solid state at all compositions despite the presence of a solid miscibility gap and eutectic reaction in the equilibrium phase diagram. Subsequent TEM examination [2,3] showed that splat quenched Ag-Cu solidified from the melt as a single solid phase free of microsegregation. However for concentrated alloys spinodal decomposition of this structure was difficult to avoid in rapid solidification experiments. Other reports of solubility extension are common especially in aluminum based alloys [4]. Frequently these alloys exhibit a cellular microsegregation pattern [5] but are occasionally found to also be free of microsegregation [6]. The present paper addresses the solidification requirements to produce microsegregation-free crystalline structures.

Experiments which pinpoint the rapid solidification conditions required to produce changes in the microstructure of alloys are difficult to perform because of the unknown aspects of the nucleation temperature in many rapid solidification techniques. Surface melting and resolidification experiments using lasers or electron beams permit better control over solidification velocity than other rapid solidification techniques.

Surface melting experiments involve no bulk undercooling due to the presence of the alloy substrate. Also, because the liquid is contained in its own solid, a knowledge of heat transfer coefficients is not required. This fact greatly increases the accuracy of heat flow models which can be used to determine the imposed solidification velocities [7]. Surface melting experiments on alloys have provided information on the refinement of the dendritic structure and changes in the microsegregation pattern [8,9]. Few have dealt with the formation of microsegregation-free structures.

Elliott, Gagliano, and Krauss [10], using a pulsed laser to melt a spot, showed that supersaturated solid solutions of Ag-Cu could be formed. The solutions, however, contained a rather unusual structure consisting of bands formed parallel to the local solidification interface. No estimates of solidification velocity were given. In a series of papers [11-13], Copley and coworkers have laser melted various alloys in the Ag-Cu system to form structures similar to those reported by Elliott et al. In these experiments the laser was scanned at a constant velocity similar to a welding pass up to 34 cm/s. The local solidification velocity is related to the scan speed by a geometrical factor describing the melt shape (discussed in more detail in a later section). No structures were reported which were free of this banded structure and the velocities at which the transitions of microstructure occur for a given alloy composition were not described.

In the present paper, a series of electron-beam surface melting experiments have been performed on Ag-rich, Ag-Cu alloys. The velocities which cause changes from dendritic or eutectic growth to microsegregation-free solidification are determined. Such direct information permits

the evaluation of existing rapid solidification models and points to areas where new models are required.

MECHANISMS OF MICROSEGREGATION-FREE SOLIDIFICATION

Two solidificaton mechanisms have been proposed to produce microsegregation-free crystalline alloys; planar growth with equilibrium solute partitioning, and partitionless solidification. The theoretical conditions required for planar growth with equilibrium partitioning were derived by Mullins and Sekerka [14] and extended by Coriell and Sekerka [15]. For growth at high velocities, surface tension provides a stabilization of the planar interface when the net heat flow is into the solid. For many alloys if the growth velocity exceeds a velocity, v_{ab}, given by

$$v_{ab} = \frac{mD(1-k_E)C_o}{k_E^2 T_m \Gamma} \quad , \tag{1}$$

and if

$$G^* = \frac{k_L G_L + k_S G_S}{k_L + k_S} > 0 \ , \tag{2}$$

the planar interface is stable and no microsegregation occurs. The parameter m is the liquidus slope, D is the liquid interdiffusion coefficient, k_E is the equilibrium partition coefficient, T_m is the pure component melting point, Γ is the ratio of the liquid solid surface tension to the latent heat per unit volume, C_o is the alloy composition, k_L and k_S are the liquid and solid thermal conductivities and G_L and G_S are the liquid and solid temperature gradients. For alloys beyond the solid solubility limit, solidification is presumed to occur on the

metastable liquidus and solidus extensions and presents no theoretical difficulty. As can be seen from Eq. (1), the velocity for planar growth is a strong function of the partition coefficient. For an alloy where k_E is relatively small ($\sim$ 0.1), planar growth does not occur unless the velocity exceeds 1 m/s for this theory. In this range of velocity the kinetics of interface motion probably become important in practice and the equilibrium partition coefficient cannot be used. For alloys where k_E is closer to unity, especially those involving surface melting where $G^*>0$, microsegregation-free structures can be produced at lower velocity by this mechanism with interfacial conditions close to equilibrium. However, a critical test of the theory is still lacking.

When the growth rate approaches the range of 1 m/s, interface kinetics are thought to significantly alter the interface partition coefficient. At this growth rate the characteristic diffusion length D/V for solidification is $\sim$ 1 nm for most liquid metals and strong deviations from interface equilibrium should be expected. Conclusive observation of a deviation from local equilibrium was first made by Baker and Cahn [16] when Zn-rich Zn-Cd alloys with compositions beyond the Zn-solidus retrograde were splat cooled into HCP structures with compositions beyond the retrograde. Hence, equilibrium partitioning was not a possibility, and the partition coefficient must have deviated from its equilibrium value. The term solute trapping is loosely applied to conditions whenever this deviation occurs, but as originally defined [16,17], is restricted to the case when the chemical potential of the solute increases during solidification. More recently, data on the velocity dependence of the partition coefficient, k, in laser melted and regrown ion implanted Si has been obtained [18-19]. Such data

generally show significant changes in the partition coefficient for these very dilute additions in the interface velocity range from 1 to 5 m/s. Various theoretical models, applicable to dilute solutions, have been proposed for the velocity dependence of the partition coefficient [20-23]. In most of these theories the partition coefficient changes sharply in the vincinity of a velocity, D/a_o, where a_o is a length scale related to interatomic dimensions.

Several of these trapping models have been employed by Coriell and Sekerka [24] in a more complete treatment of interface stability theory at high solidification rates. If the rate of change of k with velocity is not too large, the stability limit can be estimated by inserting the k for the velocity of interest into Eq. (1). When the rate of change of k with velocity is large, the theory predicts oscillatory instabilities.

A commonly discussed limiting case of solute trapping occurs when k is unity. This is called partitionless solidification (and sometimes diffusionless, massive, or complete trapping). Partitionless solidification is only possible when the interface temperature is below the T_o curve for the alloy composition for the liquid to solid transformation of interest [17]. Frequently however, partitionless solidification is associated with interface temperatures below the solidus of the average alloy composition [25]. Most detailed kinetic treatments of partitionless solidification of metallic systems [26-27] suggest that only slight undercooling ($\sim$ 10 K) below T_o should be necessary to drive a liquid-solid interface with no solute partitioning.

Various competitive growth models for partitionless solidification have been proposed for alloys of eutectic composition. Boswell and Chadwick [2] have calculated the time-temperature-transformation curves

for eutectic growth and partitionless growth using nucleation and growth concepts. They calculate a cooling rate required to avoid eutectic formation for Ag-Cu and hence promote the formation of the single phase supersaturated solution. Bec! Copley, and Bass [13] have compared the eutectic interface temperature obtained from eutectic growth theory with the T_0 temperature for the Ag-Cu eutectic composition. In this model, when the velocity of eutectic solidification would require an interface temperature below the T_0 curve, a transition to partitionless growth is suggested.

EXPERIMENTS

Ag-rich Ag-Cu alloys were chosen for the present study for several reasons. No metastable phases have been produced by rapid solidification other than the extended FCC solution phase. The phase diagram is relatively well known and has recently been fit by Murray [28] using free energy functions, thus permitting a calculation of the metastable portions of the diagram (fig. 1) along with the T_0 curve and the spinodal. The small temperature difference ($\sim$ 100 °C) between the T_0 and the stable portions of the two liquidus curves, has long been associated [29] with the extension of solubility in this system. Two additional phase diagram features are convenient. For dilute Ag-rich alloys the equilibrium partition coefficient is 0.47. This relatively high value provides the theoretical possibility of absolute interface stability at solidification velocities below those where nonequilibrium solate trapping is thought to occur. Furthermore, the metastable Ag solidus curve exhibits a calculated retrograde at 10 wt.% Cu and 700 °C. Assuming that this retrograde exists, alloys with compositions greater than 10 wt.% Cu must solidify with some degree of solute trapping when a single phase solid is produced as in the Zn-Cd experiments of Baker and Cahn [16].

Alloys were prepared for electron-beam surface melting and resolidification experiments by vacuum induction melting of 99.999 percent pure components in a graphite crucible and chill casting under argon in a carbon-coated copper slab mold. Ingots were cold-rolled to 3 mm thick sheets. For the surface melting experiments, the sheets were prepared by the following procedure to produce either no microsegregation or microsegregation fine enough to ensure complete mixing during surface melting. Alloys containing 1 and 5 wt.% Cu were homogenized for 20 h at 750 °C. Alloys containing 9, 15, and 23 wt.% Cu were surface melted using overlapping electron-beam passes to a depth of ~ 0.5 mm at a scan speed of 3 cm/s. This produces a dendrite arm spacing less than 1 μm. These sheets were then rolled slightly to eliminate surface topography produced by the e-beam melting. Alloys containing 28.1 wt.% Cu (the eutectic composition) required no pretreatment due to the fineness of the eutectic structure. Wet chemical analysis of the six alloys yielded compositions of 1.07, 5.49, 9.23, 15.25, 23.50, and 28.61 wt.% Cu. These values are considered accurate to 1 percent of the stated values.

Rapid solidification experiments were performed by single, one-dimensional sweeps of a focused 21 keV electron beam across the surface of a prepared alloy substrate which was attached to a water-cooled copper block. Ten to twelve sweeps, 3 mm apart, were conducted on a single substrate at speeds between 1.5 and 400 cm/s. The average temperature of the substrated was monitored by a thermocouple and rose by less than 10 °C for a short time after each sweep.

Because the beam focal size could not be measured directly using available techniques [30] at the high current levels required to melt Ag alloys, the following procedure was adopted. For a series of scans,

the electron beam was first visually focused to approximately 1 mm diameter. While scanning at 100 cm/s, the beam current was raised to a level ($\sim$ 50 mA) just below that where a green plasma was seen. Increases of beam current beyond this level were avoided because of the formation of a large protrusion of the alloy above the substrate surface at the weld centerline after solidification. The focus conditions were maintained constant during the passes at the various speeds and the beam current was reduced slightly (< 10%) for the slowest speeds to avoid the plasma formation. At the slow scan speeds the melted zones were typically 0.6 mm wide and 0.2 mm deep while at 400 cm/s the melted zones were typically 0.2 mm wide and 0.02 mm deep. Samples for metallography were obtained as sections transverse to the scan direction and occasionally the other two perpendicular sections. TEM samples were obtained by ion milling half disks, 3 mm in diameter, cut from 0.1 mm thick transverse slices through the weld zone. In a few cases, 0.1 mm thick slices parallel to the substrate surface were made. Disks punched from the latter were ion milled mainly from the substrate side to yield a thin area in the solidified zone near the top surface.

Significant effects arise from the change in weld puddle shape as the scan rate is increased. The local solidification velocity is equal to the product of the scan velocity with the cosine of the angle, θ, between the scan direction and the local growth direction. Because of this factor, growth velocities even at the top center of the weld puddle for high scan speeds may differ significantly from the scan speed. By examining longitudinal sections through a weld centerline by optical microscopy and assuming that grain boundaries propagate parallel to the growth direction, the angle, θ, at the top center of a weld was

Table I

Variation of Growth Direction with Scan Speed

V (cm/s)	$\frac{Va}{2\alpha}$	θ (degrees)	cosθ	Width (μm)	Depth (μm)
9	0.23	15	0.97	400	200
12	0.30	47	0.68	650	425
30	0.75	30	0.86	700	240
36	0.90	30	0.86	400	70
70	1.75	60	0.50	300	60
200	5.0	60	0.50	500	75
400	10.0	72	0.30	430	30

measured. Table I shows these measurements at various scan speeds, V, for the longitudinal sections performed in this study. Also shown in the table is a dimensionless form of the scan speed, $Va/2\alpha$ where a is the beam radius (here taken as 0.5 mm) and α is the thermal diffusivity. Kou, Hsu, and Mehrabian [7] have calculated weld puddle shapes for values of the dimensionless scan velocity less than one and for heat inputs which just avoid excessive vaporization. These calculations are thought to approximate the present experiments for scan speeds below 30 cm/s, in which range the growth velocity near the weld surface usually differs from the scan speed by 15 percent or less for the calculated shapes as well as the measured θ values. At velocities of 200 cm/s, the measurements indicated that the growth rate is about one-half of the scan speed. Clearly the exact relation of the growth rate to the scan speed depends on the exact conditions of beam input power and focal size.

RESULTS

Figure 2 shows a summary of the microstructure observed at the top center of the weld zone as a function of the electron beam scan velocity and alloy composition for all experiments performed. The figure is divided into four regions exhibiting four general types of microstructure: (a) dendritic (cellular), (b) eutectic, (c) banded, and (d) microsegregation-free. The detailed results shown in figure 2 will be described by alloy composition.

Ag-1 wt.% Cu and -5 wt.% Cu

Dilute alloys exhibit a transition from segregated to microsegregation-free structures at velocities which increase with alloy composition. Ag-1 wt.% Cu alloys were cellular at all velocities below 20 cm/s, while Ag-5 wt.% Cu alloys were cellular or dendritic below 60 cm/s. Typical cellular structures for these alloys are shown in figure 3a and 3c. At or above these velocities respectively, each alloy is free of solidification microsegregation (fig. 3b and 3d). The finest cell spacing observed in the 1 wt.% Cu alloy was $\sim$ 0.5 μm as seen in figure 3a. In this case, the cell walls were decorated with dislocations and were enriched in Cu. Typical ratios of CuKα counts to AgL counts from adjacent cell center and cell wall regions were 0.040 and 0.054 respectively. At slower growth rates increased segregation was observed but a detailed study of this phenomenon was not performed. Alloys containing 5 wt.% Cu generally were dendritic with secondary arms at velocities below 15 cm/s; but contained no secondary arms at higher speeds (fig. 3c). The finest cell spacing observed at this composition was $\sim$ 0.3 μm (not shown). The transition from dendritic to cellular structure was

not examined in detail and for the remainder of this paper no distinction will be made between cellular and dendritic structures.

Ag-9 wt.% Cu, -15 wt.% Cu, and -23 wt.% Cu

These alloy compositions are beyond the equilibrium solubility limit (8.8 wt.% Cu) of Cu in Ag at the eutectic temperature. However, the 9 wt.% Cu alloy does not exceed the Ag-solidus metastable retrograde composition. As seen in figure 2, the microstructure of each of these alloys changes with increasing velocity from dendritic to banded and from banded to microsegregation-free.

The maximum velocity at which dendritic growth is observed decreases with alloy composition from 30 cm/s for Ag-9 wt.% Cu to 3 cm/s for Ag-23 wt.% Cu (fig. 2). Figure 4 shows SEM micrographs of the dendritic structure of Ag-9 wt.% Cu alloys obtained from the free surface of the melt trails at the centerline for three velocities. The continued refinement of the primary arm spacing with scan velocity is shown in figure 5. The rate of change of spacing with the actual solidification velocity may however be somewhat different due to changes in weld puddle shape as discussed previously. TEM examination of a Ag-15 wt.% Cu melt trail scanned at 2.5 cm/s showed a cellular microsegregation pattern with a relatively small volume fraction of eutectic in some areas and no eutectic in other areas (fig. 6).

A structure consisting of light and dark etching bands or striations is observed by optical microscopy in the intermediate velocity range shown in figure 2. The existence of such bands in Ag-Cu alloys has been reported previously [10-13]. Figure 7 shows a transverse and a longitudinal section through the weld centerline for a 15 wt.% Cu alloy scanned at 30 cm/s. The lower part of the melted region, where the

solidification velocity is lowest, is dendritic. The upper part of the melted region is banded. As seen in figure 7b (and also fig. 10) the bands follow the expected shape of the trailing edge of a melted zone. A transition from dendritic to banded structure, observed within a sample, suggests strongly that the origin of the banding phenomenon is growth related rather than an artifact of nonsteady beam power [10] or melt convection [12]. A more detailed description of the banded structure is deferred until the next section.

At higher velocities the 9, 15, and 23 wt.% Cu alloys are free of the banded structure (fig. 2), and solidification produces a microsegregation-free structure. The velocity required to produce this transition decreases with increasing composition. Figure 8 shows micrographs of a 23 wt.% Cu alloy scanned at 157 cm/s. The transition from a banded structure at the bottom of the melted region, where the growth rate is low, to a band-free structure at the top of the melted region, where the growth rate is high, is seen in figure 8b. TEM micrographs of this sample (fig. 8c) confirm the absence of bands but show solid state (spinodal) decomposition of the microsegregation-free structures produced from the melt.

Ag-28 wt.% Cu and Banded Structure

Alloys of eutectic composition, when electron beam melted below 2.5 cm/s, consists of a fine eutectic structure as shown in figure 9. The minimum eutectic spacing observed is $\sim$ 20 nm. The electron diffraction pattern from the eutectic yields lattice parameters of 0.405 nm and 0.365 nm for the two phases. These values are close to those obtained [31] for Ag and Cu at their respective limits of equilibrium solid solubility at the eutectic temperature.

Above 2.5 cm/s the eutectic composition does not solidify by a coupled growth mechanism. The microstructure consists of the same banded structure observed for noneutectic alloys. Figure 10 shows longitudinal sections through the melt trail centerlines which clearly show that the bands follow the shape of the solidifying surface of the melted zone. At higher velocities the band shapes change as the molten zone shape distorts as discussed previously. In figure 10 the band spacing measured perpendicular to the bands is seen to increase slightly from the bottom of the melted zone to the top. Examination of all samples showed band spacings increasing from $\sim$ 0.8 μm to $\sim$ 1.5 μm as the growth velocity increased.

TEM examination of the banded structure (fig. 11) in a 23 wt.% Cu alloy scanned at 17 cm/s revealed alternate layers of cellular and cell-free alloy. Evidently the dark etching material seen in optical micrographs of the banded structure corresponds to the cellular layer. X-ray fluorescence measurement in the TEM with a probe size just large enough to average over the width of an individual layer ($\sim$ 0.4 μm) revealed no significant difference in average composition between the cellular and cell-free layers. Clearly lateral microsegregation does exist however within the cellular layers.

Care was taken in the preparation of the TEM sample to document the sense of growth direction. The cellular layer originates microstructurally from an interface instability occurring in the previously formed cell-free layer. The cellular structure then propagates for a short distance until a dark layer marks the cell fronts. The continuity between the cell-free layer and the subsequently formed cellular region is seen clearly by the common crystallographic orientation evident in

the isolated subgrain (dark grain) seen in figure 11a. For higher scan velocities the width of the cellular layers decreases compared to the width of the cell-free layers, until at high velocity the cellular layers disappear and the banded structure is absent. In eutectic alloys, the banded structure is identical but with a finer cell size. Microsegregation-free structures occur in the eutectic alloy when scanned at 70 cm/s and above and appear identical to figure 8.

DISCUSSION

Four major results merit discussion in the present paper:

(a) For 1 and 5 wt.% Cu alloys, a transition from cellular growth to cell-free growth occurs at velocities which increase with composition.

(b) For 9, 15, and 23 wt.% Cu alloys a transition from cellular or dendritic growth to the banded structure occurs at velocities which decrease with composition.

(c) For 28 wt.% Cu (the eutectic composition), the maximum rate achievable for coupled growth of Ag- and Cu-rich phases is 2.5 cm/s. The banded structure occurs between 2.5 cm/s and 70 cm/s.

(d) For 15, 23, 28 wt.% Cu alloys, a transition from banded growth to microsegregation-free growth occurs at high velocities ($\sim$ 1 m/s) which decrease with increasing composition.

Absolute Stability

For 1 and 5 wt.% Cu alloys, the transition from cellular to cell-free structures occurs at velocities of 15 and 60 cm/s respectively. Because these velocities are below those normally associated with solute trapping for dilute alloys, the predictions of morphological stability

theory with equilibrium partitioning at the interface were examined. Table 2 shows a summary of the relevant phase diagram parameters, diffusion coefficient, prediction of the stability theory using Eq. (1), v_{ab}, and experimental results, v_{obs}, for 1, 5, and 9 wt.% Cu alloys. Because steady state planar growth with local interface equilibrium is not possible for compositions beyond a solidus retrograde, Eq. (1) cannot be applied for compositions greater than 9 wt.%. The values for k_E and m shown are averages taken from three recent evaluations [28,32,33] and the uncertainty in the function $m(1-k_E)/k_E^2$ is shown in the table. The diffusion coefficient was assumed to depend only on temperature as given below the table [34]. Measurements of dilute Ag-Cu and Cu-Ag alloys do not suggest any strong composition dependence. The diffusion coefficient was evaluated at the solidus temperature, T_s, for each composition, corresponding to the interface temperature for a planar interface under local equilibrium conditions. The surface tension was taken as 126 ergs/cm^2 [35] and the latent heat per unit volume was taken as 1.017×10^{10} ergs/cm^3.

The calculated values of the velocity required for planar growth of the 1 and 5 wt.% Cu alloys are a factor of two higher than the experimental results. This is considered excellent agreement in view of the uncertainty of diffusion data. If the difference had increased with composition (velocity), a dependence of k on v in this velocity range might have been suggested, but no such trend was seen. The wavelengths at the onset of instability, λ_{ab}, have also been calculated [36] and are reasonably consistent with the minimum cell spacings observed, λ_{obs}. A comparison of the theory with experiment for the 9 wt.% alloy

is complicated by the occurrence of bands and the lower and upper velocity limits of the banded region are given in Table 2 for completeness.

Coupled Growth

The maximum observed growth rate for the Ag-Cu eutectic in the present work is ∿ 2.5 cm/s with a spacing of ∿ 20 nm. Cline and Lee [37] have directionally solidified the Ag-Cu eutectic up to a growth rate of 0.27 cm/s with an average lamellar spacing of ∿ 95 nm. The lamellar spacing λ and the growth velocity, v, were related by

Table II

Summary of Absolute Stability Conditions

C_o (wt.%)	k_E	m (K/wt.%)	$\frac{m(1-k_E)}{k_E^2}$ (K/wt.%)	T_s (K)	$D_L(T_s)$ (cm^2/s)	v_{ab} (cm/s)	v_{obs} (cm/s)	λ_{ab} (μm)	λ_{obs} (μm)
1	0.47	8.7	20.9± 6	1215	2×10^{-5}	27	15	0.53	∿ 0.5
5	0.41	6.8	23.9± 9	1136	1.5×10^{-5}	117	60	0.16	∿ 0.3
9	0.30	4.8	37.3±17	1043	1×10^{-5}	219	60/200	--	--

$$D = 1.22 \times 10^{-3} \text{ cms}^{-1} \exp\{-10^4 \text{ cal mole}^{-1}/RT\}$$

$$\lambda^2 v = 1.4 \times 10^{-11} \text{ cm}^3/\text{s}. \quad (3)$$

Extending their relation to a growth velocity of 2.5 cm/s predicts a lamellar spacing of 23.7 nm. However as discussed below, use of Eq. (3) in this velocity range may be invalid.

It is interesting to note that the finest spacing seen by Boswell and Chadwick [2] in splat quench Ag-Cu alloys was ∿ 30 nm. They used this observation to assess the growth rate imposed by the splat quench

on the foil. This eutectic structure occurred only in small regions adjacent to the metastable extended solid solution. Hence it seems more likely that a maximum growth rate for the eutectic was reached in the small regions and surpassed in most of the foil to form the metastable structure.

The present results strongly suggest that there exists a limit on the rate at which coupled eutectic growth can occur. One theoretical limit can be found from the effect of a temperature dependent diffusion coefficient even when local equilibrium of the interface is maintained. Inclusion of this effect in eutectic growth [38] leads to the prediction of a maximum growth rate. This phenomenon is identical to that which gives rise to C-shaped TTT curves for solid state eutectoid decomposition. However in solidification theories, the liquid diffusion coefficient is normally assumed to be temperature independent. For rapid solidification, especially of concentrated alloys, this assumption may be invalid.

Consider a phase transformation, such as eutectic growth, which follows diffusive kinetics according to

$$v = \alpha\, D(T)\, (T_E - T)^2 \tag{4}$$

where α is a constant of proportionality, D(T) is the temperature dependent diffusion coefficient and T_E is the equilibrium reference temperature for the transformation. Differentiation of Eq. (4) yields a maximum growth rate when the interface temperature T is undercooled to a critical temperature, T_c where

$$T_c = \frac{Q}{4R}\left\{\left(1 + \frac{8RT_E}{Q}\right)^{\frac{1}{2}} - 1\right\}. \tag{5}$$

Here D has been assumed to exhibit Arrhenius behavior with an activation energy of Q according to

$$D = D_o \exp\{-Q/RT\} \quad . \tag{6}$$

For the Ag-Cu eutectic with T_E = 1053 K and Q = 10 kcal/mole [34], Eq. (5) gives T_c = 799 K. To predict the maximum growth rate for the eutectic, the constant α in Eq. (4) must be known. Using the measured value of the $\lambda^2 v$ constant [37] and phase diagram information*, Eq. (17) from Jackson and Hunt [39] can be used to determine a value of $\alpha D(T_E)$ of 1.9×10^{-4} cm $s^{-1}K^{-2}$. This value is significantly smaller than other estimates [2,13] using surface energy rather than phase diagram data. The present analysis also yields a value of 2.7×10^{-4} cm K for the product $\lambda(T_E-T)$ which is independent of the diffusion coefficient. Using the relation given below Table 2 to calculate a diffusion coefficient for the eutectic composition, one obtains 1.0×10^{-5} cm^2/s at T_E and 2.2×10^{-6} cm^2/s at T_c. These considerations lead to a predicted maximum rate for coupled eutectic growth for Ag-Cu of 2.7 cm/s at an undercooling of 254 K with a eutectic spacing of 10.6 nm. Although the predicted maximum velocity agrees well with experimental results, the spacing does not. The discrepancy may be related to the assumption, $\lambda << D/v$, used by Jackson and Hunt to solve the diffusion equation. At the maximum growth rate predicted above, D/v = 8.5 nm. Hence there exists strong experimental and theoretical reasons for a limit on the

*The combined liquidus slope parameter m, is taken as 2 $K(wt.\%)^{-1}$. The difference in composition, C_o, between the solid phases (assumed independent of temperature) is taken as 83.3 wt.%. The ratio of the widths of the Cu and Ag lamellae measured from replicas [37] is taken as 1/3.

eutectic growth rate in the range of 1 to 10 cm/s. Such a limit calls into question the careless extrapolation of $\lambda^2 v$ relations.

It should be emphasized that the temperature dependence of the liquid diffusion coefficient only becomes important in the present analysis because of the relatively large undercoolings required to accomplish the solute redistribution and surface area creation necessary for eutectic growth. For dilute alloys this effect is much less important.

A second explanation, which has been suggested as a limit on the eutectic growth rate, involves a comparison of the eutectic interface temperature to the T_0 temperature for the alloy [13,38]. In this model, when the imposed growth rate of the eutectic requires an interface temperature below T_0, the alloy will prefer the partitionless mode of solidification. However, objections to this approach exist. The undercooling required for eutectic growth which is discussed here is a consequence of diffusion difficulties and liquid-solid interface curvature, under conditions of local equilibrium. In eutectic growth, the liquid at the interface in front of each growing phase is much different from the eutectic composition. For partitionless solidification, the interface temperature must be below the T_0 temperature for the liquid composition at the interface. This can never happen in a kinetic model which assumes local equilibrium.

Dendritic Growth

A temperature dependent diffusion coefficient also leads to a maximum rate for dendritic growth of concentrated alloys. Although the theory of alloy dendritic growth is continually being refined especially for high rate [40], a simple expression formulated by Burden and Hunt for controlled growth [41] demonstrates the qualitative features of the

composition dependence of this maximum rate for dendritic growth. For high growth rate (or zero temperature gradient) an expression for the velocity and temperature of a dendrite tip is identical to Eq. (4) with T_E replaced by T_L, the liquidus temperature for the bulk alloy composition. In this case, α is inversely proportional to the alloy composition if the liquidus slope, partition coefficient and surface tensions are independent of composition. Equation (5) can be used to find T_c, the critical tip temperature for the maximum growth rate. The value of α given by Burden and Hunt contains numerical factors inconsistent with stability theory.* In consideration of this fact, a value of α for dendrites has been selected which makes the velocity of dendritic growth of the eutectic composition equal the velocity of eutectic growth. The value for α for dendrites cannot be larger than this because of the existence of a symmetric coupled zone for this alloy [42].†

Table III shows calculated values of the critical dendrite tip temperature for the maximum velocity of dendritic growth for various Ag-Cu alloy compositions. This calculated maximum velocity decreases with increasing composition and roughly parallels the experimental data for the boundary between dendritic and banded microstructure. For very dilute alloys this maximum is irrelevant because it occurs at velocities where a planar interface is stable.

An alternate idea which one could propose to predict a maximum growth rate for alloy dendrites would be to assess the velocity at

---

*The growth velocity when the dendrite tip temperature equals the solidus temperature for the bulk alloy composition should agree with the velocity required for absolute stability of a planar interface.

†Competitive growth models of the coupled zone determine the range of composition and temperature where eutectic growth is faster than dendritic growth [43].

which the tip temperature reaches the T_o curve. This idea is analogous to the similar idea proposed for the eutectic and is rejected for the same reason.

Table III

Maximum Rate for Dendritic Growth

C_o (wt.%)	T_L (K)	T_c (K)	T_L-T_c (K)	$D(T_c)$ (cm^2/s)	v_{max} (cm/s)	$v_{max}^{observed}$ (cm/s)
28.1	1053	799	254	2.2×10^{-6}	2.7	2.5
23	1085	818	267	2.7×10^{-6}	4	4
15	1136	849	288	3.4×10^{-6}	10	15
9	1176	872	304	3.9×10^{-6}	20	45

$$v = \alpha\, D(T_c)(T_L-T_c)^2 \qquad \text{where} \qquad \alpha = \frac{5.3\times10^{2}\,cm^{-1}K^{-2}(wt.\%)}{C_o}$$

Microsegregation-Free Structure

Because the banded structure is eliminated at velocities of the order of 1 m/s, the transition from banded structure to microsegregation-free structure is most likely related to nonequilibrium solute trapping. The upper velocity boundary of the banded region (Fig. 2) when extrapolated to pure Ag suggests a velocity for solute trapping of $\sim$ 5 m/s for dilute alloys. This velocity is consistent with data obtained for solute trapping in dilutely doped Si [18-19]. There would be, of course, no microstructural indication of solute trapping in the 1 and 5% Cu alloys at 5 m/s because microsegregation-free structures become possible at lower velocity due to the absolute stability mechanism.

The fact that the eutectic composition can be produced as a single phase microsegregation-free material at lower growth rates than, for example, 9, 15, and 23 wt.% Cu alloys suggests a significant composition dependence for the onset of solute trapping. The solute trapping models mentioned earlier in this paper [20-23] involve no explicit concentration dependence. A simple approach to include a composition dependence in a trapping theory would be to employ the diffusion coefficient at the T_o temperature for the various compositions into these trapping models. At the melting point of pure silver, the diffusion coefficient is 2×10^{-5} cm^2/s [34]. For the eutectic composition the T_o temperature is approximately 940 K and the diffusion coefficient, based on an activation energy of 10 kcal/ mole, is 6×10^{-6} cm^2/s. This simple idea leads to the conclusion that the growth velocity required for significant levels of solute trapping would be reduced by a factor of three as the composition changes from pure Ag to the eutectic composition. Such a trend is consistent with the observed data. Furthermore a recently refined model of solute trapping in concentrated alloys also predicts a decrease in the velocity required for solute trapping for concentrated Ag-Cu alloys [44].

This composition dependence is however inconsistent with the usual idea invoked in rapid solidification that the magnitude of the temperature difference between the liquidus and the solidus or the temperature difference between the liquidus and the T_o curve determines the magnitude of the "cooling rate" to achieve partitionless solidification.

The observation of microsegregation-free structure for these concentrated alloys does not rigoriously guarantee that solidification occurred in a partitionless manner. However because of the solidus

retrograde, nonequilibrium must have occurred at the interface. The possibility, thought to be unlikely, remains that the partition coefficient may not have been unity in these cases. Only future experiments carefully designed to measure directly the partition coefficient can answer this question.

Banded Structure

The origins of the banded structure, apparently unique to Ag-Cu alloys, are difficult to determine with certainty. The observation of a change with increasing growth rate from dendritic growth to banded structure and from banded structure to microsegregation-free structure observed from the bottom to top of individual weld zones is important. It precludes nongrowth related phenomena such as convection or beam power "spikes" as the cause of the banding. Beck, Copley, and Bass [13] have recently suggested that the bands are due to an instability proposed by Baker and Cahn [17] related to growth with interface temperatures above the solidus. The observation of band-free structures at high velocity in alloys with composition beyond the Ag-solidus retrograde, where single phase Ag growth must occur "above" the Ag solidus, seems to negate this idea. However, the presence of the retrograde itself appears not to be essential for the banding since the 9 wt.% Cu alloy exhibits the same microstructural trends as do more concentrated alloys.

The oscillatory interface instability predicted by Coriell and Sekerka [24] for planar growth in the velocity range where the partition coefficient is rapidly changing from the equilibrium value to unity provides another possible mechanism for the formation of the bands.

Such an instability however would cause a three dimensional microsegregation pattern; i.e., the normal two dimensional cellular microsegregation pattern modulated in addition in the growth direction. The observed banded structure does not fit this pattern. However, it is important to note that the bands are caused by alternating changes in microstructure from planar to cellular growth as solidification progresses.

The preceding discussion has suggested that the lower and upper velocity boundaries of the banded region in figure 2 are caused respectively by a limitation of the maximum growth rate of dendritic or eutectic growth in concentrated alloys and by a significant deviation from interfacial equilibrium and the concommitant increase of the partition coefficient to unity. Clearly the microscopic events which occur during the formation of the banded structure must be related to these two phenomena.

A possible sequence of microscopic events during solidification of the banded structure is as follows. Consider an initially cellular structure growing at its maximum velocity. If the imposed growth rate exceeds this maximum, the tips of the cellular interface will begin to lag behind the motion of the isotherms. As the cellular interface gets farther behind, a liquid zone of the same composition as the average alloy forms which is well below the T_o temperature. (Note: $T_c \ll T_o$). At some instant, solid of composition equal to the liquid forms and a flat interface races forward in a partitionless manner to catch up with the advancing isotherms. As the interface catches up to the isotherms, the interface velocity drops, partitioning begins to occur, the interface breaks down into cells and the process repeats itself.

CONCLUSIONS

(1) For Ag-1 and 5 wt.% Cu alloys the transition from cellular to cell-free structure occurs at velocities which increase with composition and which are consistent with the predictions of the absolute stability branch of the morphological stability theory of the liquid-solid interface.

(2) For Ag-9, 15, 23, and 28 wt.% Cu alloys a maximum growth rate exists beyond which dendritic or for the 28 wt.% Cu alloy, eutectic growth cannot occur. This maximum growth rate decreases with increasing composition (2.5 cm/s at the eutectic composition) and appears related to the difficulty of solute redistribution in conjunction with the temperature dependence of the liquid diffusion coefficient.

(3) Beyond this maximum velocity, a nonsteady state solidification process produces a banded structure consisting of alternate layers of cellular and cell-free alloy perpendicular to the growth direction.

(4) At velocities of the order of 1 m/s, which generally decrease with increasing composition, microsegregation-free structures are formed for alloys from 9 to 28 wt.% Cu. These results suggest that the growth velocity for significant solute trapping is composition dependent.

ACKNOWLEDGMENT

The authors acknowledge the support of DARPA for this research. The authors are extremely grateful to Charles H. Brady for the metallographic preparation and to John W. Cahn, Sam R. Coriell, and Robert Mehrabian for many helpful discussions.

REFERENCES

[1] P. Duwez, R. H. Willens, and W. Klement, Jr.: J. Appl. Phys., 1960, vol. 31, p. 1136.

[2] P. G. Boswell and G. A. Chadwick: J. Mat. Sci., 1977, vol. 12, p. 1879.

[3] R. Stoering and H. Conrad: Acta Met., 1969, vol. 17, p. 933.

[4] H. Jones: Aluminum, 1978, vol. 54, p. 274.

[5] H. Jones: Matl. Sci. & Eng., 1969/70, vol. 5, p. 1.

[6] P. Furrer and H. Warlimont: Z. Metallkunde, 1973, vol. 64, p. 236.

[7] S. Kou, S. C. Hsu, and R. Mehrabian: Met. Trans. B, 1981, vol. 12B, p. 33.

[8] R. Kadalbal, J. Montoya-Cruz, and T. Z. Kattamis: Rapid Solidification Processing Principles and Technologies, II, R. Mehrabian, B. H. Kear and M. Cohen, eds. p. 195, Claitor's, Baton Rouge, LA, 1980.

[9] B. G. Lewis, D. A. Gilbert, and P. R. Strutt: Rapid Solidification Processing Principles and Technologies, II, R. Mehrabian, B. H. Kear and M. Cohen, eds. p. 221, Claitor's, Baton Rouge, LA, 1980.

[10] W. A. Elliott, F. P. Gagliano, and G. Krauss: Met. Trans., 1973, vol. 4, p. 2031.

[11] S. M. Copley, M. Bass, E. W. Van Stryland, D. G. Beck, and O. Esquivel: Proc. III Int. Conf. Rapidly Quenched Metals, B. Cantor, ed. Vol. 1, p. 147, The Metals Society, London, 1978.

[12] D. G. Beck, S. M. Copley, and M. Bass: Met. Trans. A, 1981, vol. 12A, p. 16.

[13] D. G. Beck, S. M. Copley, and M. Bass: Met. Trans. A, 1982, vol. 13A, p. 1879.

[14] W. W. Mullins and R. F. Sekerka: J. Appl. Phys., 1964, vol. 35, p. 444.

[15] S. R. Coriell and R. F. Sekerka: Rapid Solidification Processing Principles and Technologies, II, R. Mehrabian, B. H. Kear and M. Cohen, eds. pp. 35-49, Claitor's, Baton Rouge, LA, 1980.

[16] J. C. Baker and J. W. Cahn: Acta Met., 1969, vol. 17, p. 575.

[17] J. C. Baker and J. W. Cahn: Solidification, p. 23, ASM, Metals Park, OH, 1971.

[18] P. Baeri, G. Foti, D. M. Poate, S. V. Campisano, and A. G. Cullis: Appl. Phys. Lett., 1981, vol. 38, p. 800.

[19] C. W. White, B. R. Appleton, B. Stritzker, D. M. Zehner, and S. R. Wilson: Laser and Electron Beam Solid Interactions and Materials Processing, p. 59, North Holland, NY, 1981.

[20] J. C. Baker: Interfacial Partitioning During Solidification, Ph.D. Thesis, Chapter V, MIT, 1970. Also reported by J. W. Cahn, S. R. Coriell, and W. J. Boettinger: Laser and Electron Beam Processing of Materials, p. 89, Academic Press, NY, 1980.

[21] M. J. Aziz: J. Appl. Phys., 1982, vol. 53, p. 1158.

[22] K. A. Jackson, G. H. Gilmer, and H. J. Leamy: Laser and Electron Beam Processing of Materials, p. 104, Academic Press, NY, 1980.

[23] R. F. Wood: Phys. Rev., 1982, vol. B25, p. 2786.

[24] S. R. Coriell and R. F. Sekerka: J. Crystal Growth, 1983, vol. 61, p. 499.

[25] see for example, K. Löhberg and H. Müller: Z. Metallkunde, 1969, vol. 60, p. 231.

[26] M. Hillert and B. Sundman: Acta Met., 1977, vol. 25, p. 11.

[27] W. J. Boettinger, S. R. Coriell and R. F. Sekerka: Third Conference on Rapid Solidification Processing, held at NBS in December 1982; R. Mehrabian, Chairman.

[28] J. L. Murray: National Bureau of Standards, Washington, DC, unpublished research, 1983.

[29] B. Giessen and R. H. Willens: The Use of Phase Diagrams in Ceramics, Glass, and Metal Technology, p. 103, vol. 3, Academic Press, NY, 1970.

[30] R. J. Schaefer, W. J. Boettinger, F. S. Biancaniello, and S. R. Coriell: Lasers in Metallurgy, p. 43, TMS-AIME, Warrendale, PA, 1981.

[31] R. K. Linde: J. Appl. Phys., 1966, vol. 37, p. 934.

[32] B. Giessen: Bull. of Alloy Phase Dia., 1980, vol. 1, no. 1, p. 41.

[33] J. H. Perepezko: Univ. of Wisconsin, Madison, WI, unpublished research, 1983.

[34] T. Yamamura and T. Ejima: J. Japanese Inst. Met., 1973, vol. 37, p. 901.

[35] J. H. Holloman and D. Turnbull: Prog. Met. Phys., 1953, vol. 4, p. 333.

[36] S. R. Coriell: National Bureau of Standards, Washington, DC, unpublished research, 1983.

[37] H. E. Cline and H. Lee: Acta Met., 1970, vol. 18, p. 315.

[38] W. J. Boettinger: Rapidly Solidified Amorphous and Crystalline Alloys, p. 15, Elsevier, 1982.

[39] K. A. Jackson and J. D. Hunt: TMS-AIME, 1966, vol. 236, p. 1129.

[40] R. Trivedi: Iowa State University, Ames, Iowa, unpublished research, 1983.

[41] M. H. Burden and J. D. Hunt: J. Cryst. Growth, 1974, vol. 22, p. 109.

[42] B. L. Jones, G. M. Weston, and R. T. Southin: J. Cryst. Growth, 1971, vol. 10, p. 313.

[43] M. H. Burden and J. D. Hunt: J. Cryst. Growth, 1974, vol. 22, p. 328.

[44] M. J. Aziz: Third Conference on Rapid Solidification Processing held at National Bureau of Standards in December 1982; R. Mehrabian, Chairman.

FIGURE CAPTIONS

1. Ag-Cu phase diagram [28]. Dotted lines are metastable boundaries, dashed line is the T_o curve and the dash-dot curve is the spinodal. Note the metastable retrograde in the Ag solidus.

2. Summary of microstructures observed in Ag-Cu alloys as a function of composition and electron-beam scan velocity. Open circles denote microsegregation-free structures, solid circles denote cells or dendrites, crosses denote banded structures, and triangles denote eutectic structure.

3. (a) Cellular and (b) cell-free structures obtained in Ag-1 wt.% Cu alloys rapidly solidified at 10 and 20 cm/s respectively. (c) Cellular and (d) cell-free structures obtained in Ag-5 wt.% Cu alloys rapidly solidified at 30 and 60 cm/s respectively TEM.

4. Refinement of primary dendrite arm spacing with scan velocity for Ag-9 wt.% Cu alloys. SEM. (a) 3 cm/s, (b) 6 cm/s, and (c) 15 cm/s.

5. Plot of primary dendrite spacing versus electron beam scan velocity for Ag-9 wt.% Cu. At velocities above 60 cm/s the structure is not dendritic.

6. Cellular microsegreation pattern observed in Ag-15 wt.% Cu alloy at a scan velocity of 2.5 cm/s. TEM. Note the general absence of eutectic except in the upper right corner.

7. (a) Transverse and (b) longitudinal sections of an Ag-15 wt.% Cu alloy scanned at 30 cm/s, showing transition from (unresolved) dendritic structure to the banded structure. Optical microscopy. The scan direction is to the right in (b).

8. Microsegregation-free structure obtained in Ag-23 wt.% Cu scanned at 157 cm/s. Note the presence of the banded structure at the bottom of the weld zone in (b) and the presence of spinodal decomposition in (c). (a,b) optical microscopy, transverse sections (severely etched); (c) TEM.

9. Fine eutectic structure observed in an Ag-28.1 wt.% Cu sample scanned at 2.5 cm/s. The eutectic spacing is $\sim$ 20 nm.

10. Longitudinal sections of Ag-28.1 wt.% Cu alloy scanned at 9 cm/s. Electron beam scan direction is to the right.

11. TEM micrographs of the banded structure in Ag-15 wt.% Cu alloy scanned at 17 cm/s. Nominal growth direction is from lower right to upper left. The bands consist of layers of cellular and cell-free material.

FIGURE CAPTIONS

1. Ag-Cu phase diagram [28]. Dotted lines are metastable boundaries, dashed line is the T_o curve and the dash-dot curve is the spinodal. Note the metastable retrograde in the Ag solidus.

2. Summary of microstructures observed in Ag-Cu alloys as a function of composition and electron-beam scan velocity. Open circles denote microsegregation-free structures, solid circles denote cells or dendrites, crosses denote banded structures, and triangles denote eutectic structure.

3. (a) Cellular and (b) cell-free structures obtained in Ag-1 wt.% Cu alloys rapidly solidified at 10 and 20 cm/s respectively. (c) Cellular and (d) cell-free structures obtained in Ag-5 wt.% Cu alloys rapidly solidified at 30 and 60 cm/s respectively TEM.

4. Refinement of primary dendrite arm spacing with scan velocity for Ag-9 wt.% Cu alloys. SEM. (a) 3 cm/s, (b) 6 cm/s, and (c) 15 cm/s.

5. Plot of primary dendrite spacing versus electron beam scan velocity for Ag-9 wt.% Cu. At velocities above 60 cm/s the structure is not dendritic.

6. Cellular microsegreation pattern observed in Ag-15 wt.% Cu alloy at a scan velocity of 2.5 cm/s. TEM. Note the general absence of eutectic except in the upper right corner.

7. (a) Transverse and (b) longitudinal sections of an Ag-15 wt.% Cu alloy scanned at 30 cm/s, showing transition from (unresolved) dendritic structure to the banded structure. Optical microscopy. The scan direction is to the right in (b).

8. Microsegregation-free structure obtained in Ag-23 wt.% Cu scanned at 157 cm/s. Note the presence of the banded structure at the bottom of the weld zone in (b) and the presence of spinodal decomposition in (c). (a,b) optical microscopy, transverse sections (severely etched); (c) TEM.

9. Fine eutectic structure observed in an Ag-28.1 wt.% Cu sample scanned at 2.5 cm/s. The eutectic spacing is $\sim$ 20 nm.

10. Longitudinal sections of Ag-28.1 wt.% Cu alloy scanned at 9 cm/s. Electron beam scan direction is to the right.

11. TEM micrographs of the banded structure in Ag-15 wt.% Cu alloy scanned at 17 cm/s. Nominal growth direction is from lower right to upper left. The bands consist of layers of cellular and cell-free material.

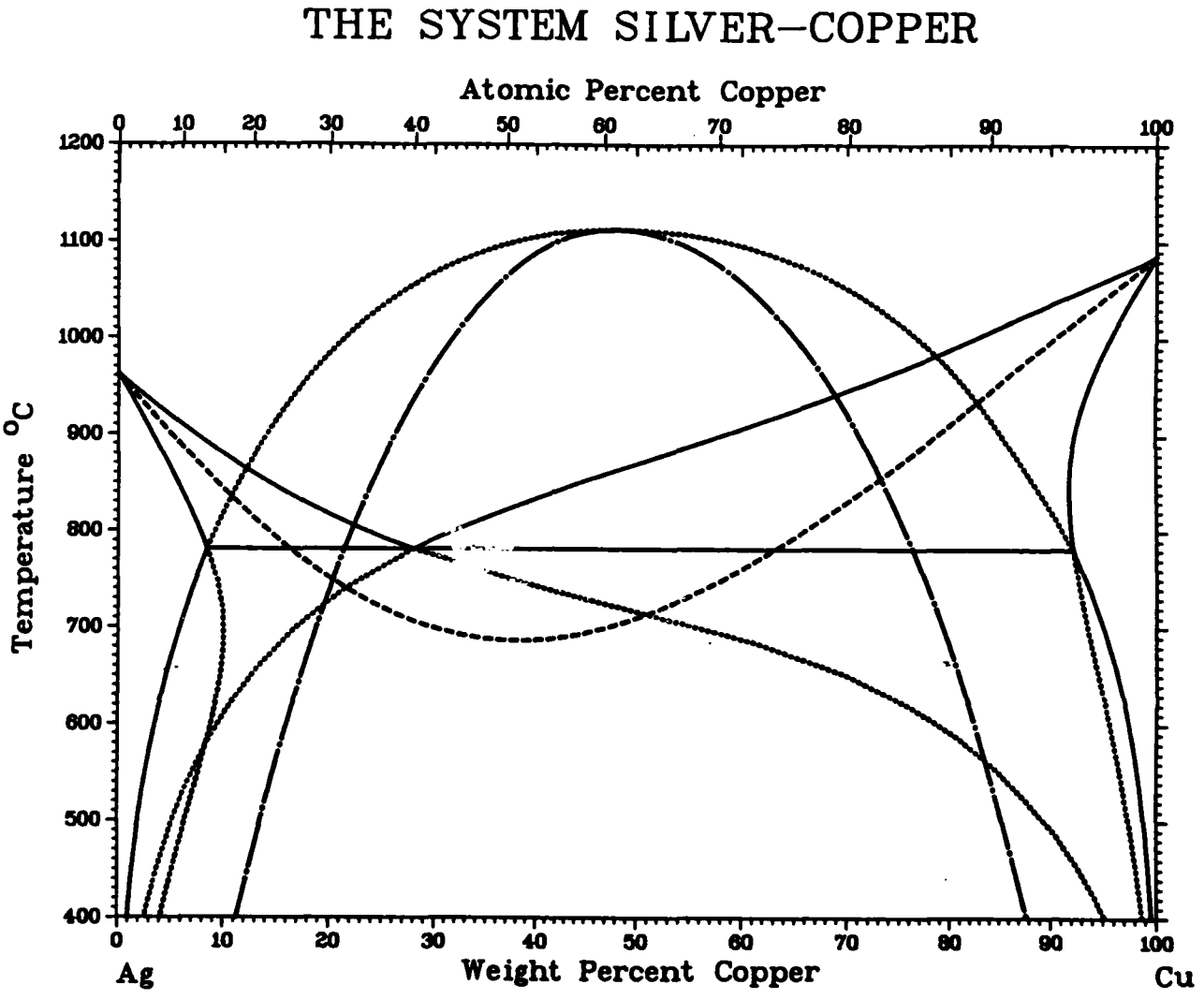

1. Ag-Cu phase diagram [28]. Dotted lines are metastable boundaries, dashed line is the T_o curve and the dash-dot curve is the spinodal. Note the metastable retrograde in the Ag solidus.

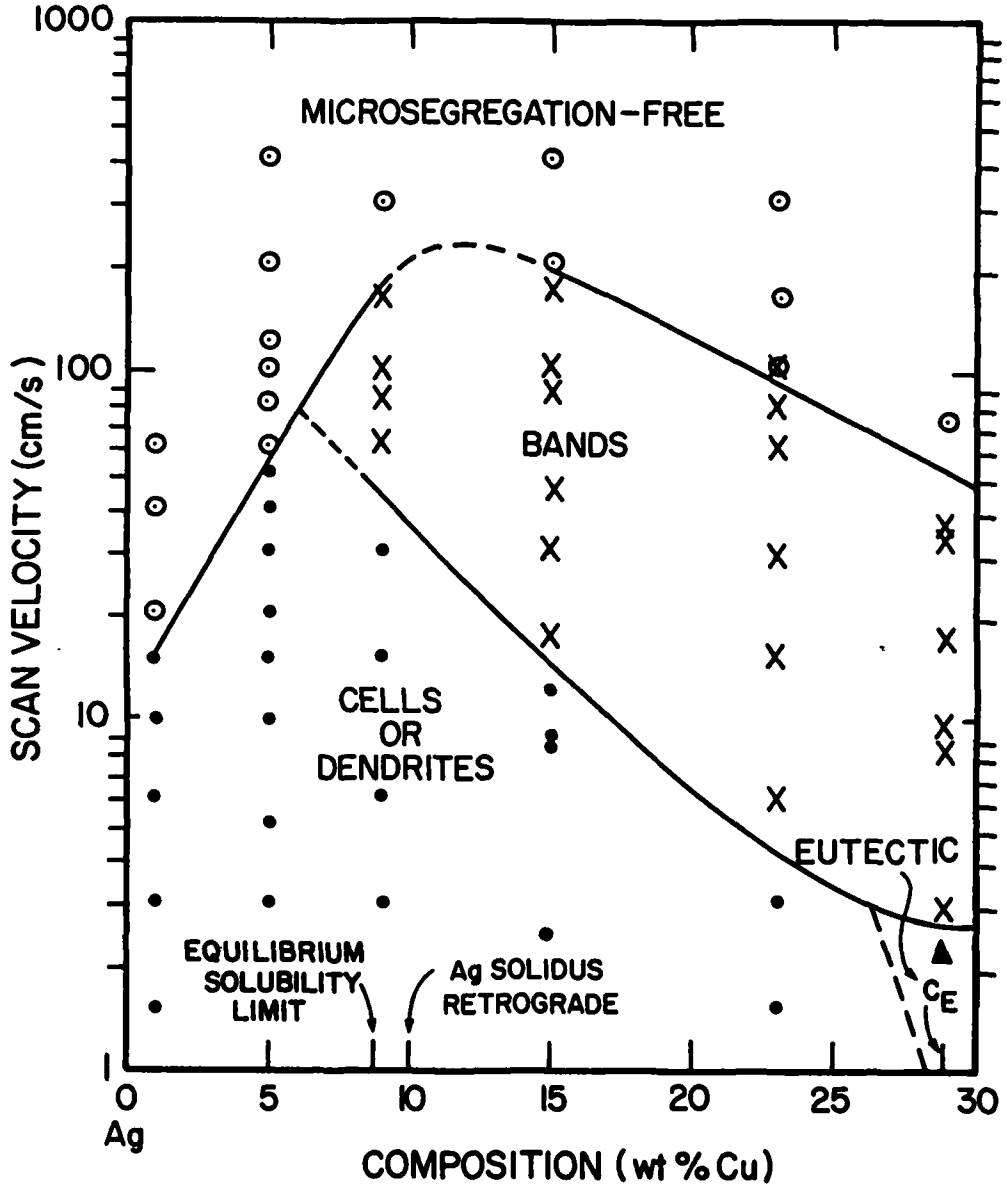

2. Summary of microstructures observed in Ag-Cu alloys as a function of composition and electron-beam scan velocity. Open circles denote microsegregation-free structures, solid circles denote cells or dendrites, crosses denote banded structures, and triangles denote eutectic structure.

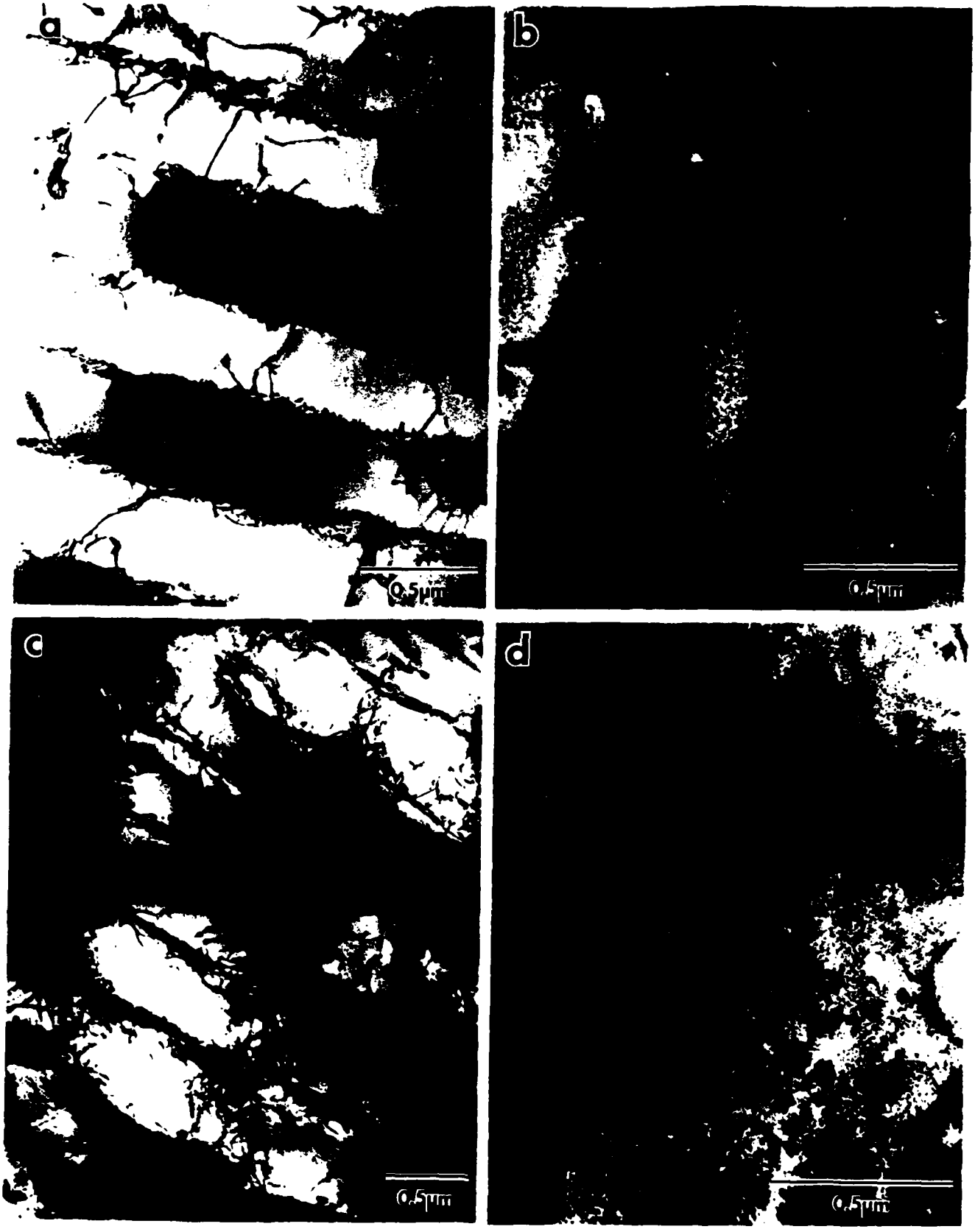

3. (a) Cellular and (b) cell-free structures obtained in Ag-1 wt.% Cu alloys rapidly solidified at 10 and 20 cm/s respectively. (c) Cellular and (d) cell-free structures obtained in Ag-5 wt.% Cu alloys rapidly solidified at 30 and 60 cm/s respectively. TEM.

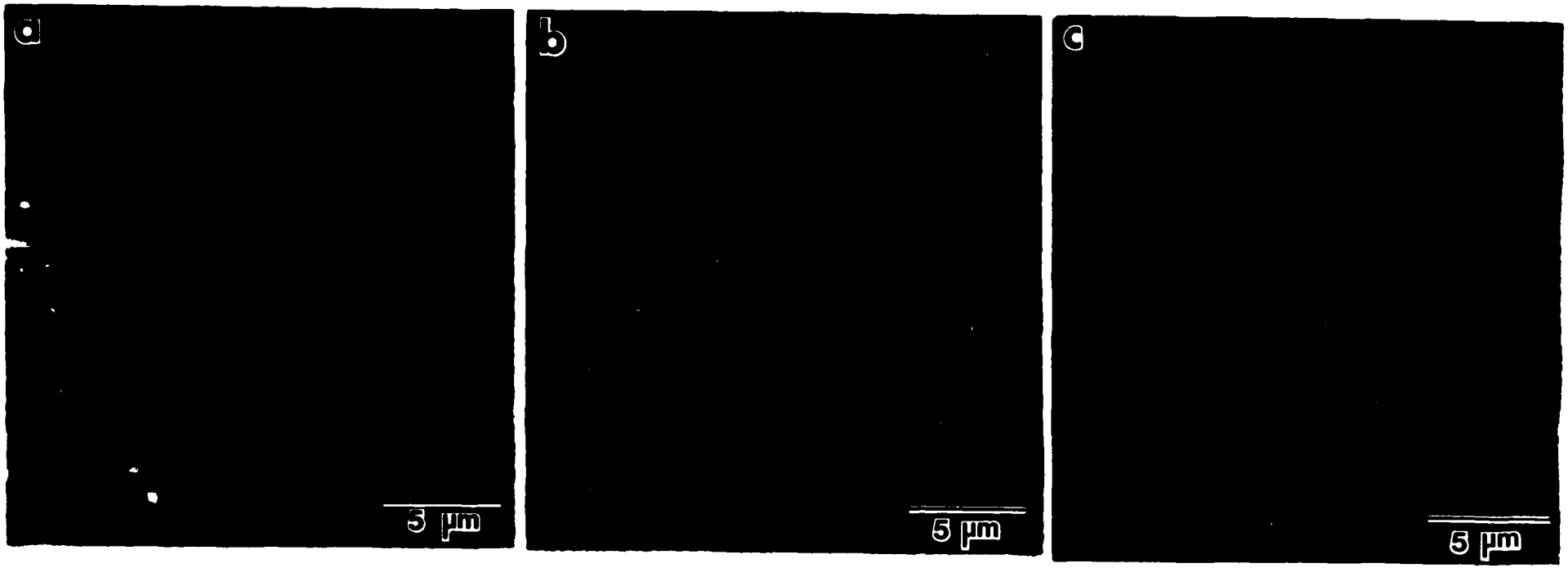

4. Refinement of primary dendrite arm spacing with scan velocity for Ag-9 wt.% Cu alloys. SEM. (a) 3 cm/s, (b) 6 cm/s, and (c) 15 cm/s.

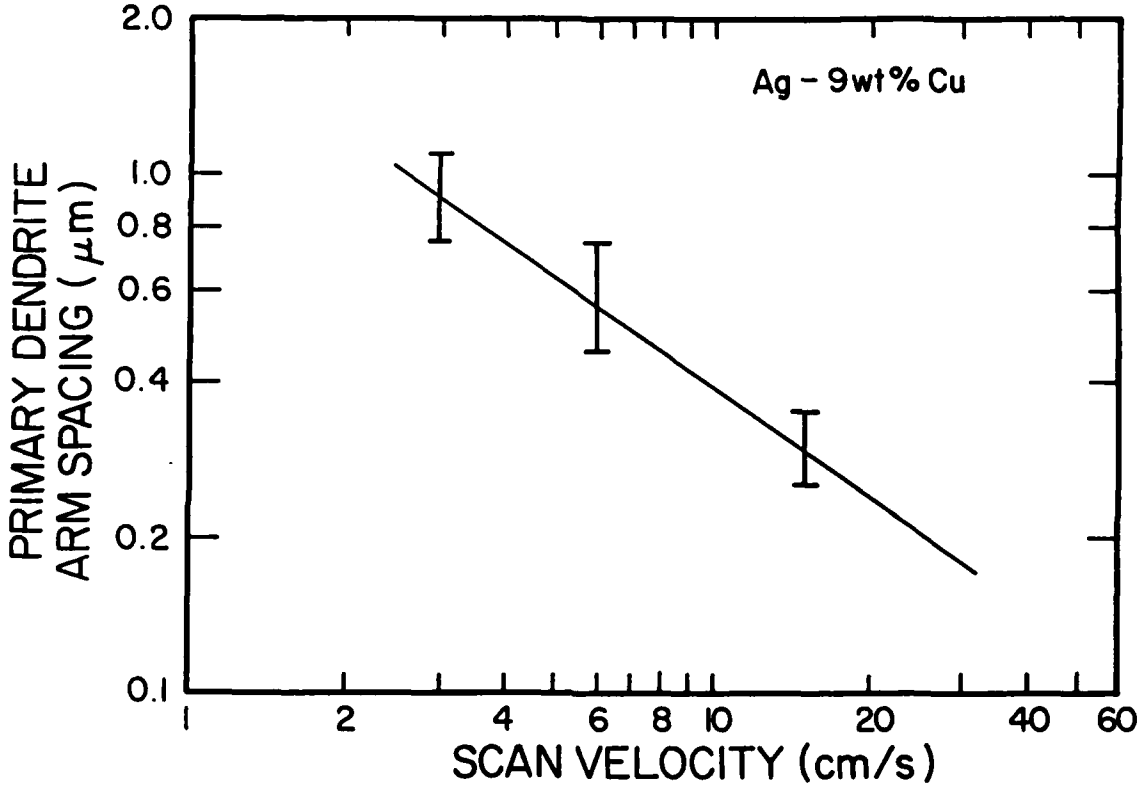

5. Plot of primary dendrite spacing versus electron beam scan velocity for Ag-9 wt.% Cu. At velocities above 60 cm/s the structure is not dendritic.

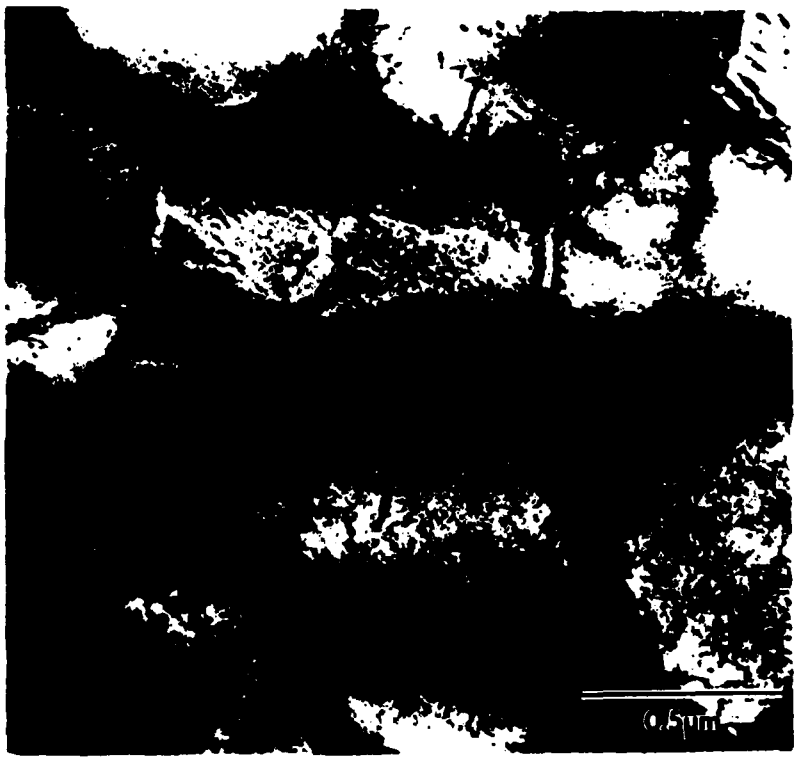

6. Cellular microsegreation pattern observed in Ag-15 wt.% Cu alloy at a scan velocity of 2.5 cm/s. TEM. Note the general absence of eutectic except in the upper right corner.

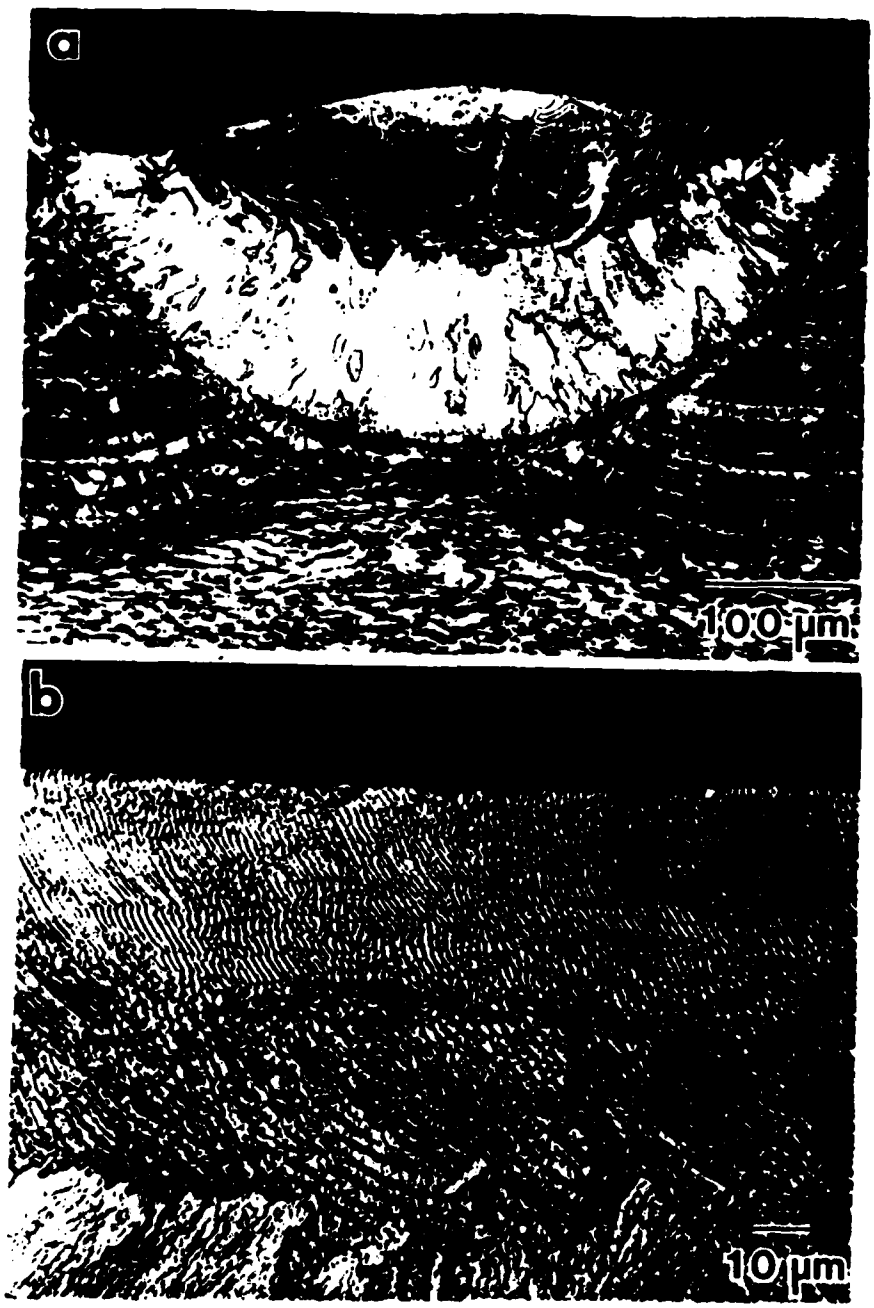

7. (a) Transverse and (b) longitudinal sections of an Ag-15 wt.% Cu alloy scanned at 30 cm/s, showing transition from (unresolved) dendritic structure to the banded structure. Optical microscopy. The scan direction is to the right in (b).

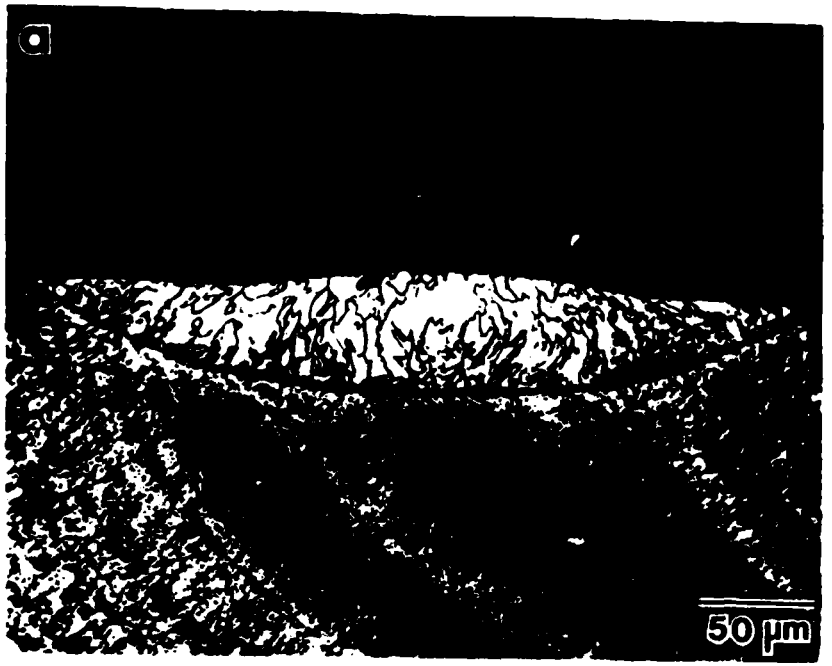

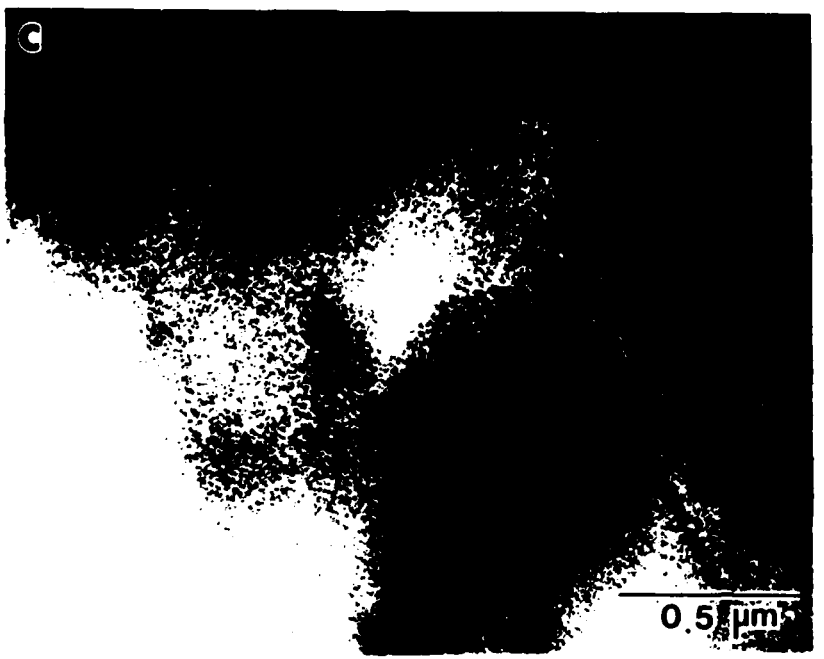

8. Microsegregation-free structure obtained in Ag-23 wt.% Cu scanned at 157 cm/s. Note the presence of the banded structure at the bottom of the weld zone in (b) and the presence of spinodal decomposition in (c). (a,b) optical microscopy, transverse sections (severely etched); (c) TEM.

9. Fine eutectic structure observed in an Ag-28.1 wt.% Cu sample scanned at 2.5 cm/s. The eutectic spacing is ~ 20 nm.

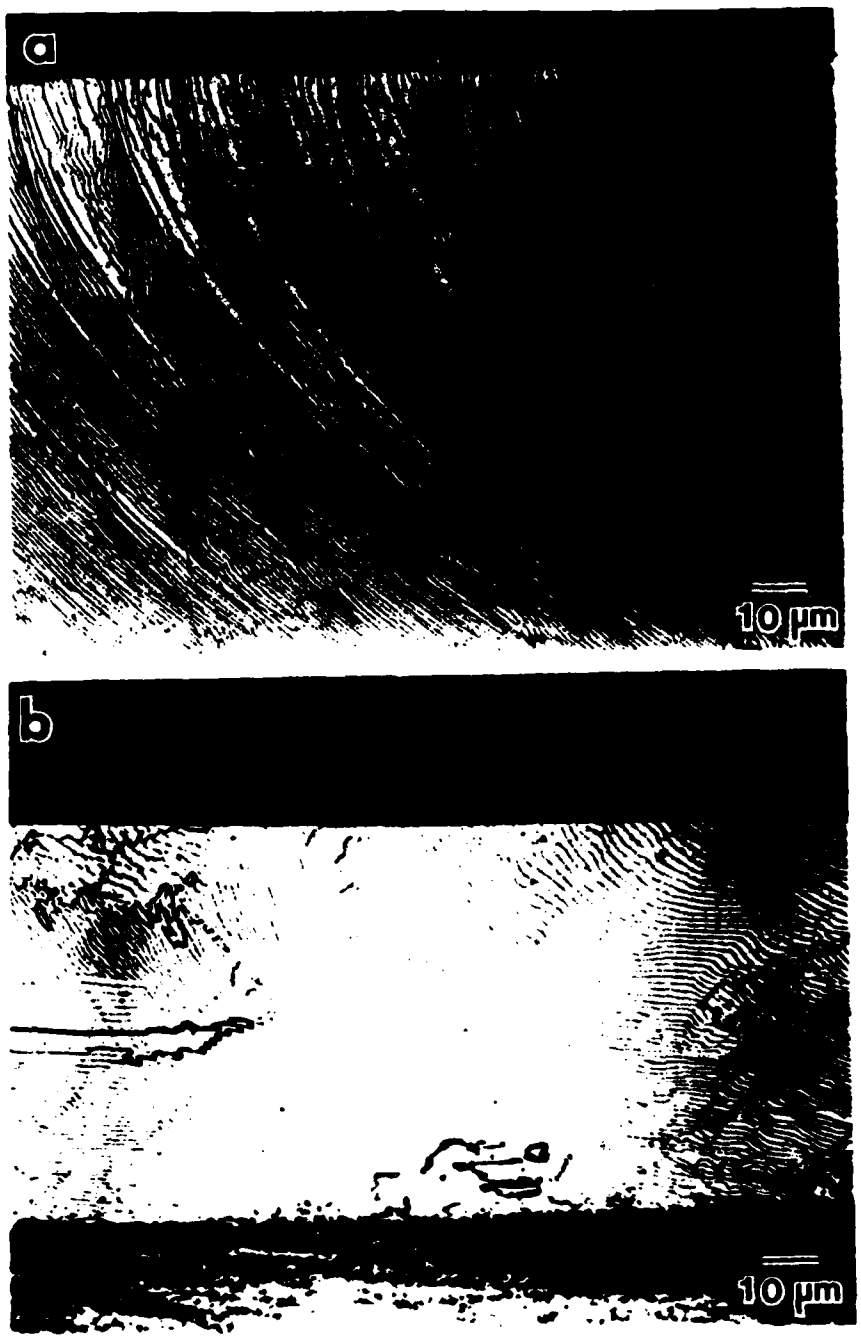

10. Longitudinal sections of Ag-28.1 wt.% Cu alloy scanned at (a) 9 cm/s and (b) 36 cm/s. Electron beam scan direction is to the right.

11. TEM micrographs of the banded structure in Ag-15 wt.% Cu alloy scanned at 17 cm/s. Nominal growth direction is from lower right to upper left. The bands consist of layers of cellular and cell-free material.

Published in Acta Metallurgica 32, 749-756 (May 1984).

MICROSTRUCTURE AND PHASE SOLUBILITY EXTENSION IN RAPIDLY SOLIDIFIED NiAl-Cr QUASIBINARY EUTECTIC

D. Shechtman*, W. J. Boettinger++,

T. Z. Kattamis+, and F. S. Biancaniello++

*Dept. of Materials Engineering
Technion, Haifa, Israel
on leave at the
Center for Materials Research
The Johns Hopkins University
Baltimore, MD 21218

+Dept. of Metallurgy
University of Connecticut
Storrs, CT 06268

++Metallurgy Division
National Bureau of Standards
Washington, DC 20234

ABSTRACT

The microstructure of melt-spun ribbon of the NiAl-Cr quasibinary eutectic composition has been characterized by optical and transmission electron microscopies. The eutectic composition is Ni-33at%Al-34at%Cr and is of interest because of the similarity of crystal structures (CsCl for β-NiAl and BCC for α-Cr) and lattice parameters of the two phases in the eutectic. The rapidly quenched microstructure consists of 0.5 μm diameter columnar grains with a composition near that of the eutectic. These grains exhibit a fine spinodal decomposition structure. Based on the presence of coarse antiphase domains within the columnar grains it is concluded that they originally formed from the melt as supersaturated β-NiAl. Between the grains a fine rod-type eutectic structure of the β-NiAl and α-Cr phases is observed with eutectic spacings as fine as 12 nm. A solidification model for the appearance of a supersaturated β-NiAl phase near the eutectic composition, rather than a supersaturated α-Cr phase, is presented based on the T_0 curves for this alloy system.

INTRODUCTION

One of the first rapidly solidified alloys that was systematically examined was the Ag-Cu eutectic system (1). Solubility extension of the terminal solid solutions was anticipated because of their identical crystal structures and similar lattice parameters (~12%). Under rapid solidification conditions the alloy can exhibit complete solubility extension across the equilibrium miscibility gap eventhough subsequent spinodal decomposition of the solidified phase is difficult to suppress (2). Subsequent examination (3,4) of thermodynamic factors which describe the possibility of solubility extension led to a relatively straightforward rationale for the behavior of this alloy system.

These thermodynamic factors are summarized by the T_o curve for the liquid to solid transformation. The T_o curve is the locus of temperatures and compositions where the molar free energies of the liquid and solid phases are equal. It represents the highest temperature, as a function of composition, at which liquid can thermodynamically transform to solid without change of composition. This type of solidification is called partitionless solidification. For liquid to solid transformations of metals, especially those involving relatively simple crystal structures, the additional kinetic undercooling required below T_o for partitionless solidification is thought to be small (5,6). Hence, T_o curves are extremely useful in assessing the possibilities for solubility extension during rapid solidification of many alloys.

The present paper reports the microstructure of melt spun ribbons of NiAl-Cr quasibinary eutectic composition and discusses the nature of the thermodynamic restrictions on solubility extension in this alloy system. This alloy is only slightly more complex than the Ag-Cu system described

above. The NiAl-Cr quasibinary section of the Ni-Al-Cr ternary system (7) contains all of the tie-lines and can therefore be treated as a true binary system between the components NiAl and Cr. The two solid phases in the quasibinary system are α-Cr and β-NiAl with BCC and ordered BCC (B2 or CsCl) structures, respectively. Both phases in the eutectic structure of this alloy have nearly identical lattice parameters (8) and differ crystallographically only by ordering. Because of these factors, significant solubility extension was anticipated. Of particular interest is to determine which phase extends its solubility most readily in response to rapid solidification.

The directional solidification of NiAl-Cr quasibinary eutectic alloy (Ni-33at%Al-34at%Cr) was previously investigated by Walter, et al. (8-11) and Lemkey (12). The eutectic consists of fine, nonfaceted fibers of α-Cr phase embedded in a β-NiAl matrix. From previous work by Kornilov and Mintz (7) the NiAl-Cr quasibinary eutectic temperature is 1445 °C. The α-Cr phase at 1200 °C was estimated to contain 20.6 mole% NiAl and, hence, has a composition of 17.1at%Ni-17.1at%Al-65.8at%Cr. The β-NiAl phase at 1200 °C was estimated to contain 84.5 mole% NiAl, hence has a composition of 45.8at%Ni-45.8at%Al-8.4at%Cr. The volume fraction of fibers is about 0.34. In the directionally solidified eutectic all directions and planes of the two phases are parallel. The solidification microstructure consists of eutectic colonies of α-fibers of circular cross-section embedded in <100> -oriented grains of β-NiAl parallel to the growth direction, except near the boundaries where they are inclined to this direction. Despite this inclination the crystallographic relationship between fibers and matrix remains the same (8). The small mismatch in lattice parameters between phases is evidenced by the large distance between dislocations observed at the interphase interface. Walter and Ciine (9) also studied the effect of growth velocity on inter-fiber spacing.

EXPERIMENTAL PROCEDURE

Rapidly solidified ribbons of NiAl-Cr quasibinary eutectic were melt-spun on a room temperature wheel in a helium atmosphere. Ribbons about 25 μm thick and 2.5 mm wide were obtained at a linear velocity of ∿24 m/s. The ribbons were studied by optical microscopy, X-ray diffraction and analytical electron microscopy. Specimens for electron microscopy were electropolished and studied in a scanning transmission electron microscope equipped for energy dispersive X-ray analysis. Composition analysis was performed at 120 kV on specimens less than 40 nm thick as determined by the $(110)_{NiAl}$ thickness fringes. The spectra were corrected for the in-hole count and stripped of the fitted background.

RESULTS

The microstructure of an arc-melted chill-cast cylindrical specimen, 6.3 mm in diameter is illustrated in Figure 1. The rod-like α-Cr phase is embedded in β-NiAl matrix.

The microstructure of the rapidly solidified ribbons as observed by optical microscopy is relatively uniform across the ribbons and consists mainly of columnar grains parallel to the heat flow direction. The intergranular spaces were not optically resolved. The average columnar grain width increased slightly with distance from the chill, Figure 2, from about 0.5 to 1.3 μm. The average columnar grain width also increased slightly with ribbon thickness.

The microstructure of a typical area of the ribbon as observed by electron microscopy is shown in Figure 3, which represents cross-sections of columnar grains that grew perpendicular to the ribbon surface. The columnar grains average 0.5 μm in diameter and are surrounded by a fine eutectic. The boundary between a columnar grain and a region of particularly fine eutectic is shown at a higher magnification in Figure 4. The

columnar grain is decomposed into a fine microstructure typical of spinodal decomposition with an average wavelength of 10 nm (lower right, Figure 4). Selected area diffraction patterns taken from the spinodally decomposed grains did not contain any detectable satellites, such as those observed in other spinodally decomposed structures (13). The absence of satellites is most probably due to the isotropy of decomposition in this system which results in diffused rings around fundamental reflections that are difficult to observe. Similar observations were previously made in the Fe-Al system (14). The uniformity of the spinodal structure across columnar grains suggests a general absence of a composition variation across the grains. The eutectic rods grow roughly perpendicular to the columnar grains and their spacing ranges from 12 nm, Figure 4, to 60 nm, Figure 3.

The microstructure as observed by electron microscopy is not uniform throughout the ribbon. In some areas the volume fraction of the intergranular eutectic is much smaller than shown in Figure 4 and the structure of the alloy is composed almost entirely of the decomposed columnar grains, Figure 5. In these areas the average composition of the columnar grains must be very close to the composition of the melt prior to solidification, i.e., the eutectic composition. In other regions of the same foil the volume fraction of the eutectic is much higher, Figure 6. These variations may correspond to local differences in solidification rate, however this was not confirmed in the present study. Despite these diferences the spinodal structures in the various columnar grains are quite similar.

A large number of columnar grains are single ordered domains. However, some of them contain two or more domains. Anti-phase domain boundaries (APB) are shown in Figures 3 and 7. APBs are not normally observed in conventionally prepared β-NiAl presumably due to the high coarsening rate of the antiphase domains. In rapidly quenched β-NiAl, however,

coarsening times are shorter and APBs can be retained in the microstructure for this reason. These APBs run across the grain and in most cases end in a chromium-rich rod of the eutectic. The significance of these APBs to the understanding of the solidification process will be discussed later in this paper.

A diffraction pattern taken from a columnar grain, Figure 8, identified the structure as CsCl (B2). A diffraction pattern taken from a columnar grain and its surrounding eutectic, Figure 9, shows no extra reflections besides the CsCl. This indicates that both phases in the eutectic and the columnar grain have the same orientation and almost identical lattice parameters. An X-ray diffraction scan taken from the ribbon shows that the diffraction peaks from the CsCl lattice and those from the BCC lattice are indistinguishable. Lattice parameter measurements resulted in a figure of a = 0.28882 nm. Convergent beam diffraction patterns were taken from a rod and the adjacent matrix of the eutectic, as shown in Figure 10. The rod is identified as BCC, Figure 10a, the matrix as CsCl structure, Figure 10b. Because of the fineness of the eutectic, the convergent beam could not be aimed at the matrix alone. Figure 10b contains therefore some intensity contribution from adjacent BCC rods. This may explain the observation that the intensity of the (200) reflection is stronger than that of the (100).

The composition analysis of the phases in the ribbon by energy dispersive analysis is complicated by the fineness of the microstructure, the absorption of the AlKα x-rays and the possibility of oxide formation (15) on the surface of electropolished foils. The last two effects cause an estimated uncertainty of 3-5 atomic percent for foils less than 40 nm in thickness near the eutectic composition. Nonetheless a qualitative confirmation of the degree of solubility extension of the β-NiAl columnar grains can be made.

Figure 11 shows raw x-ray spectra from four regions of the melt-spun ribbons. Figures 11a and b, which are quite similar, are from columnar grains in regions of the ribbon like those shown in Figures 5 and 3, respectively. Figures 11c and d are from the β-NiAl phase and the α-Cr phase, respectively from the sample shown in Figure 1. The high degree of solubility extension present in the columnar grains beyond the near equilibrium phase compositions of a more slowly cooled sample is evident.

In order to estimate the size of the composition difference between columnar grains in the various regions typified by Figures 11a and b, the following approach was used. As previously described some regions of the ribbon consist almost entirely of columnar grains and hence their composition is very close to the nominal (quasibinary eutectic) composition of the alloy. Using these regions as a standard, the composition of other columnar grains in regions of the ribbon containing significant amounts of intergranular eutectic were measured. Results from five different columnar grain regions (all less than 40 nm thick) are within ~2 at% of the eutectic composition. This difference is smaller than the estimated uncertainty of the measurements. For the discussion therefore, it will be assumed that all of the columnar grains have a composition very close to the eutectic composition.

DISCUSSION

Two features of this rapidly solidified structure are unique and will be discussed separately: The columnar grains of spinodally decomposed alloy with the CsCl structure and with composition near the eutectic, and the extremely fine rod-type eutectic structure. It is important for the analysis of rapid solidification processes to establish whether the supersaturated β-NiAl phase was a direct product of solidification or whether it has ordered in the solid state from a supersaturated α-Cr phase.

T_0 Curves

Because of the extension of solubility required for the formation of the columnar grains, an examination of the possible T_0 curves for the NiAl-Cr system is in order. Figure 12 shows the stable phase diagram as solid lines (7) and a possible schematic set of metastable extensions of the solvus curves (dashed) and the T_0 curves (long-short dashed). The figure assumes that the two solvus curves meet at a metastable tricritical point above which the transition from the BCC phase to the CsCl phase is second order. This transformation can be second order according to the symmetry restrictions of Landau (16). The proposed metastable tricritical point is thermodynamically identical to the stable tricritical point in the Fe-Al system where the ordering is between Fe (BCC) and FeAl (B2) (14). The schematic free energy curves for the solid phases shown in Figure 12 are identical to those proposed by Allen and Cahn (14). With the addition of the liquid free energy curve to generate the stable eutectic phase diagram, the structure of the T_0 curves becomes apparent. The dotted curve is the metastable extension of the second order phase transition below the tricritical point and is the locus of points where the free energy curves of the disordered and ordered phases join tangentially. This curve is thought to lie much closer to the solvus for the disordered phase rather than that for the ordered phase (17). The T_0 curve for the disordered phase is seen to split into two branches when it crosses this dotted line. The lower branch is the continuation for the disordered phase, while the upper branch is for β-NiAl phase. This upper branch continues to the NiAl side of diagram where it is the normal T_0 curve for β-NiAl.

The metastable extension of the solvus curves upward to the tricritical point, where the crystal structures differ by an ordering reaction, is formally similar to the metastable extension of the solvus curves between identical crystal structures (FCC) in the Ag-Cu system upward to an ordinary

critical point. The continuity of the T_0 curve across the phase diagram is also similar to that in Ag-Cu. Without better equilibrium solvus data it is difficult to estimate the tricritical temperature. The similarity of lattice parameters, as well as the relatively large equilibrium solubility ($\sim$15 mole%) of the two phases for each other suggest a low tricritical temperature. In analogy with the Ag-Cu system a low critical temperature would give rise to T_0 curves situated only slightly below the eutectic temperature.

Columnar Grains

Figure 12 leads to two important conclusions which are consistent with the experimental results. A first conclusion is that at the eutectic composition the T_0 curve for β-NiAl phase occurs at a higher temperature than the T_0 curve for the α-Cr phase. Hence, at the eutectic composition partitionless solidification of the β-NiAl phase can occur thermodynamically with less undercooling than that required for the partitionless solidification of the α-Cr phase. Due to the cubic crystal structures of α-Cr and β-NiAl phases no significant differences should exist in the interface attachment kinetics. Hence, the formation of supersaturated β-NiAl of eutectic composition should be favored over that of supersaturated α-Cr by rapid solidification.

A second conclusion from Figure 12 is that, if β-NiAl phase was formed with the eutectic composition directly from the melt, it would undergo subsequent solid state spinodal decomposition into ordered and disordered phases. This type of spinodal has been termed a conditional spinodal (14). Typical decomposition structures of FeAl by conditional spinodal show coarse antiphase domains of FeAl along with a fine scale compositional separation into disordered Fe and ordered phase (Figure 6, ref. 14). On the contrary, decomposition of a supersaturated disordered phase is typi-

fied by fine scale compositional separation with an antiphase domain size determined by the scale of the compositional separation (Figure 9, ref. 14). The observed structure of the columnar grains with coarse antiphase domains in the present work strongly suggests that supersaturated β-NiAl formed directly from the melt. This is also consistent with the predictions of the T_o curve stated above.

Eutectic Structure

The solidification of the ribbon is envisioned in two steps: First, the formation of the columnar grains of supersaturated β-NiAl by partitionless solidification followed by the formation of a fine rod eutectic structure in the regions between the columnar grains. This eutectic solidification would presumably result from the reduction in growth rate caused by the evolution of latent heat during growth of columnar grains. The nucleation of the BCC phase on the columnar grains seems to be difficult and is demonstrated by the fact that in most cases the eutectic originating from one columnar grain impinges directly upon an adjacent columnar grain. Only rarely do eutectics originating from adjacent grains meet. Once the eutectic has nucleated it consumes the liquid that remains between the two columns. Furthermore, the formation of the α-Cr phase of the intergranular eutectic at the intersection of the APBs of the columnar grains with the liquid-solid interface seems reasonable based on the disordered (BCC) nature of the APBs themselves.

Although a wide variety of eutectic spacings are seen ranging from 60 nm down to 12 nm the minimum spacings are of particular interest. The appearance of fine eutectic structures with spacings in the range of 20-30 nm has been reported for several rapidly solidified alloys (2,18). These values of the eutectic spacing, λ, are frequently employed with a $\lambda^2 v$ constant determined from directional solidification experiments to estimate

the solidification velocity, v, that prevails in various rapid solidification techniques. However, in the present case as well as other cases (2) the fine eutectic is observed in the same foil adjacent to an extended solubility phase. Most likely the fine eutectic formed at lower velocity than the rest of the foil, possibly after recalescence. In fact, these fine spacings are consistent with the hypothesis of a maximum allowable rate for coupled eutectic growth of about 10 cm/s (19). This maximum is caused by the inclusion of the temperature dependence of the diffusion coefficient into the eutectic growth theory. Experimentally the maximum growth rate of the Ag-Cu eutectic was shown to be about 2.5 cm/s corresponding to a spacing of 20 nm (20).

Cline and Walter (9) have measured the rod spacings, as a function of solidification velocity up to 0.21 cm/s for NiAl-Cr. They found these parameters to be related by $\lambda^2 v = 7 \times 10^{-12} cm^3/s$, deduced from their graph. The value of the $\lambda^2 v$ constant for NiAl-Cr is smaller than for Ag-Cu (1.4×10^{-11} cm^3/s) and other eutectics (21), presumably because of the low interface energy between β-NiAl and α-Cr phases. This low interface energy can be attributed to the strong orientation relation and similarity of lattice parameters of the two phases in the eutectic. The small value of $\lambda^2 v$ for NiAl-Cr may explain why this system exhibits a finer eutectic spacing at its maximum growth rate than other eutectic systems. Future experimental determination of the maximum growth rate of NiAl-Cr eutectic is planned, using electron beam remelting and self-quenching.

SUMMARY

Conventionally solidified Ni-33at%Al-34at%Cr quasibinary eutectic alloy consists of two phases which have similar crystal structures (CsCl for β-NiAl and BCC for α-Cr) and lattice parameters. The microstructure of melt-spun ribbon of this alloy consists of 0.5μm diameter columnar grains

of a composition near that of the eutectic. These grains contain coarse antiphase domains and exhibit a fine spinodal decomposition-like structure. The intergranular spaces are occupied by a fine eutectic consisting of α-Cr rods exhibiting spacings as fine as 12nm, embedded in a β-NiAl matrix. The formation of a supersaturated β-NiAl phase of eutectic composition from the melt which subsequently decomposes spinodally, rather than a supersaturated α-Cr phase is rationalized on the basis of the T_o curves for this alloy system.

ACKNOWLEDGMENTS

Thanks are due to Dr. Frank Lemkey for pointing out to WJB the similarity of phases in this alloy system and to Dr. John W. Cahn for interpretation of ordered structures. The authors are grateful to DARPA for supporting this work.

REFERENCES

1. P. Duwez, R. H. Willens and W. Klement, Jr., J. Appl. Phys. 31, 1136 (1960).
2. P. G. Boswell and G. A. Chadwick, J. Mater. Sci. 12, 1879 (1977).
3. J. C. Baker and J. W. Cahn, in Solidification, ASM Metals Park, Ohio, p. 23 (1971).
4. B. Giessen and R. H. Willens, in The Use of Phase Diagrams in Ceramics, Glass and Metal Technology, vol. 3, ed. by A. M. Alper, Academic Press, New York, p. 103 (1970).
5. M. Hillert and B. Sundman, Acta Met. 25, 11 (1977).
6. W. J. Boettinger, S. R. Coriell and R. F. Sekerka, in Rapid Solidification Processing: Principles and Technologies (III), ed. by R. Mehrabian, N.B.S. Int. Rpt. (1983).
7. I. I. Kornilov and R. C. Mintz, Dokl. Akad. Nauk. USSR 94, 1085 (1954).

8. J. L. Walter, H. E. Cline and E. F. Koch, Trans. TMS-AIME, 245 (1969) 2073.

9. J. L. Walter and H. E. Cline, Met. Trans., 1 (1970) 1221.

10. H. E. Cline and J. L. Walter, Met. Trans., 1 (1970) 2907.

11. J. L. Walter and H. E. Cline, Met. Trans., 4 (1973) 33.

12. F. Lemkey, unpublished research.

13. V. Daniel and H. Lipson, Proc. Roy. Soc., A181 368 (1943).

14. S. M. Allen and J. W. Cahn, Acta Met., 24 (1976) 425.

15. J. M. Brown, M. H. Loretto and H. L. Fraser, Analytical Electron Microscopy, R. H. Geiss, ed., San Francisco Press, 1981, p. 61.

16. L. D. Landau and E. M. Lifshitz, Statistical Physics, Pergamon Press, London, 1958, p. 434.

17. S. M. Allen and J. W. Cahn, in Alloy Phase Diagrams, ed. by L. H. Bennett, T. B. Massalski and B. C. Giessen, Elsevier (1983).

18. M. H. Burden & H. Jones, J. Inst. Metals 98, (249) 1970.

19. W. J. Boettinger, Rapidly Solidified Amorphous and Crystalline Alloys, B. H. Kear, B. C. Giessen and M. Cohen, ed., Elsevier Publishing Company, 1982, p. 15.

20. W. J. Boettinger, R. Schaefer, F. Biancaniello and D. Shechtman, Met. Trans. A, in press.

21. W. Kurz and D. J. Fisher, International Metals Reviews, Nos. 5 and 6 (1979) 177.

FIGURE CAPTIONS

Figure 1: As-cast microstructure of arc-melted NiAl-Cr quasibinary eutectic (TEM).

Figure 2: Columnar grains im melt-spun ribbon, edge-on section (optical microscopy).

Figure 3: Transverse section of columnar grains and surrounding eutectic in melt-spun ribbon (TEM). Note APBs in center grain.

Figure 4: Columnar grain-eutectic interface. Inter-rod eutectic spacing: 12nm (TEM).

Figure 5: Region of foil consisting primarily of columnar grains (TEM).

Figure 6: Region of foil consisting primarily of eutectic (TEM).

Figure 7: High magnification illustration of APBs (TEM) using (100) operating reflection under a two beam condition. (a) Bright field image and (b) dark field image.

Figure 8: Selected area diffraction (SAD) pattern of a columnar grain.

Figure 9: Diffraction pattern taken from a columnar grain and its surrounding eutectic.

Figure 10: (a) Microdiffraction from rod in eutectic. (b) Microdiffraction of matrix in eutectic.

Figure 11: Energy dispersive x-ray spectra obtained from a) a columnar grain in a region containing no eutectic; b) a columnar grain from a region containing intergranular eutectic; c) the β-NiAl phase in slowly cooled eutectic and d) the α-Cr phase in slowly cooled eutectic.

Figure 12: (a) NiAl-Cr phase diagram (solid lines), metastable extension of solvus curves (dashed) to tricritical point and T_o curves (long-short dashed) for α-Cr and β-NiAl. (b) Schematic free energy vs composition curves for NiAl-Cr system at temperatures T_1 and T_2, respectively. The short lines are the tangent points and the bold dots are the T_o points.

Fig 1

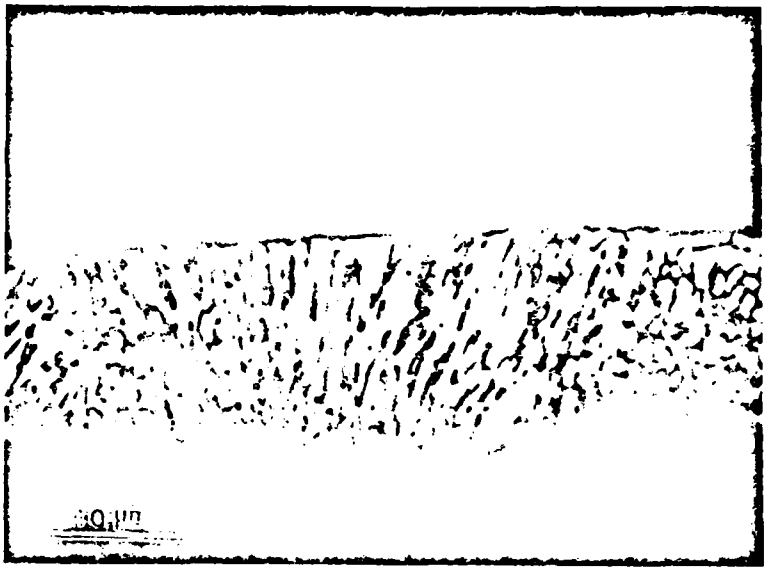

Fig 3

Fig. 4

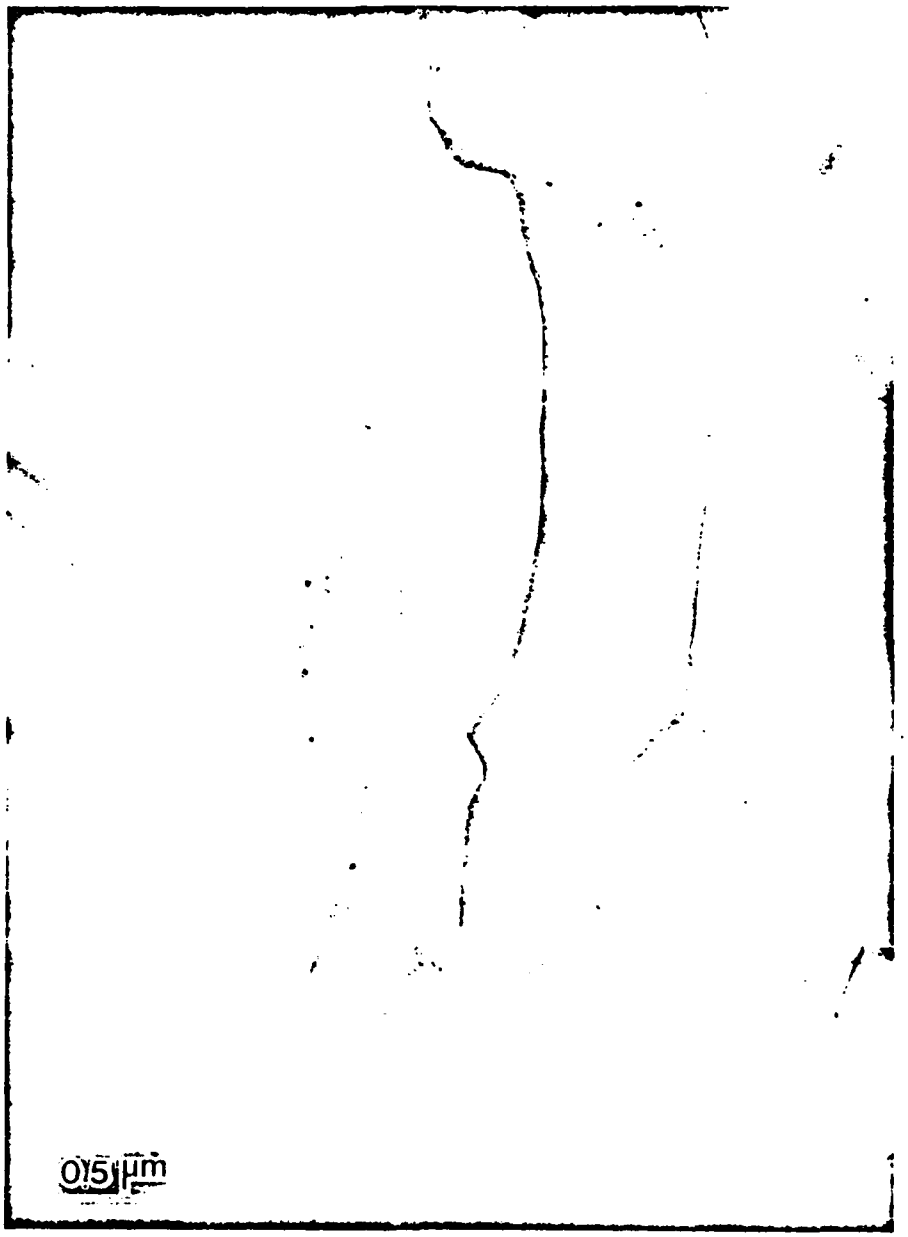

Fig. 5


0.2 μm

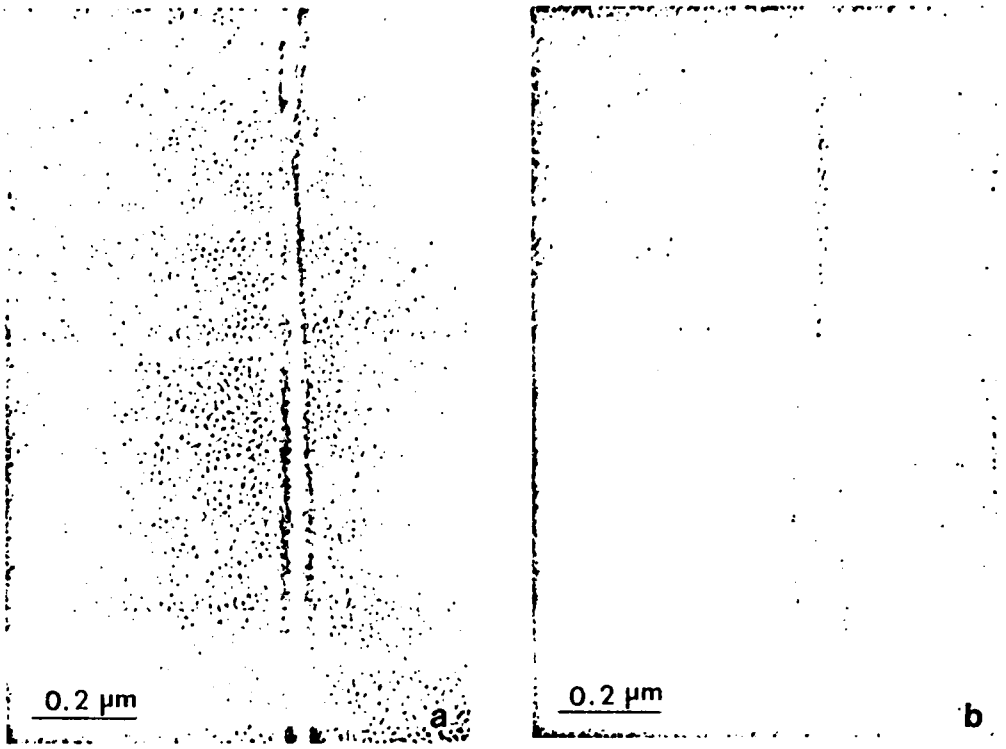
0.2 μm
a
0.2 μm
b

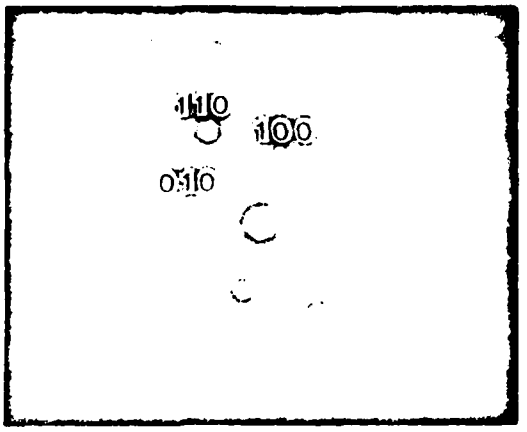

Fig. 8.

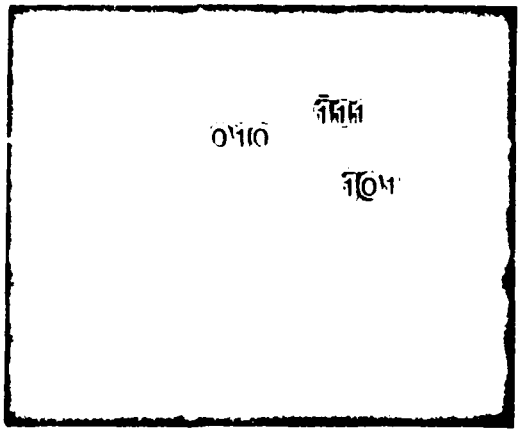

Fig 9.

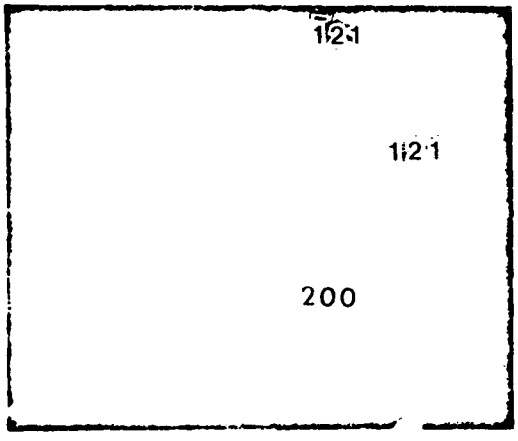

(a)

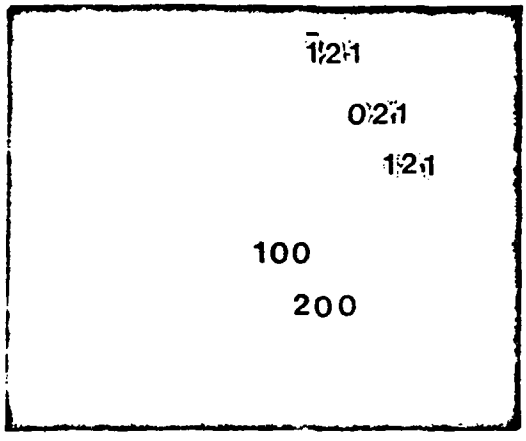

(b)

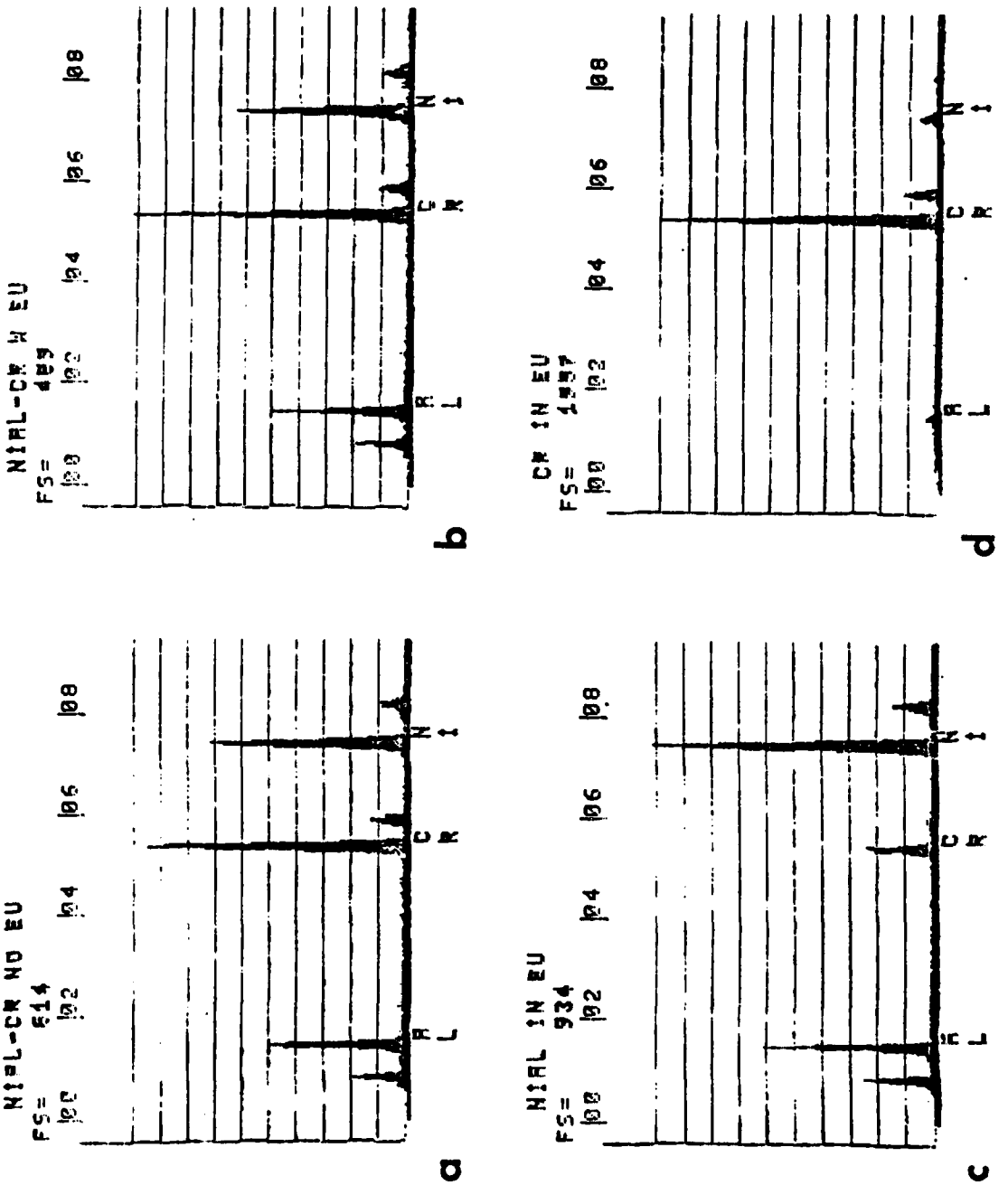
NIAL-CM ND EU
FS= 614
00 02 04 06 08
R L
C R
N 1
a
NIAL-CM W EU
FS= 489
00 02 04 06 08
R L
C R
N 1
b
NIAL IN EU
FS= 934
00 02 04 06 08
R L
C R
N 1
c
CM IN EU
FS= 1337
00 02 04 06 08
R L
C R
N 1
d

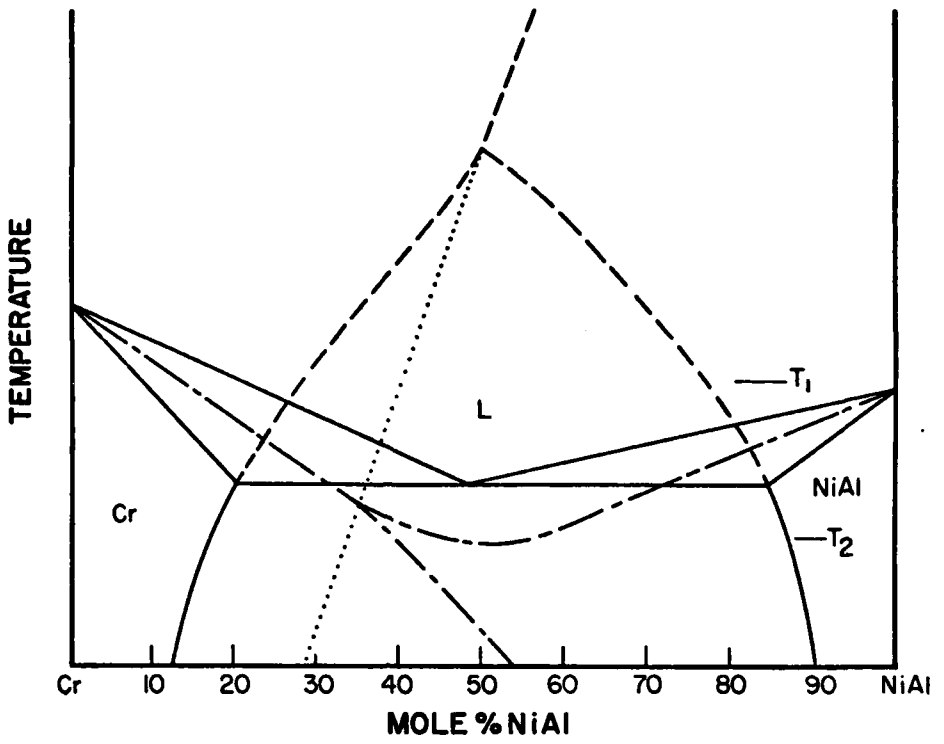
TEMPERATURE
L
T_1
Cr
NiAl
T_2
Cr
10
20
30
40
50
60
70
80
90
NiAl
MOLE % NiAl

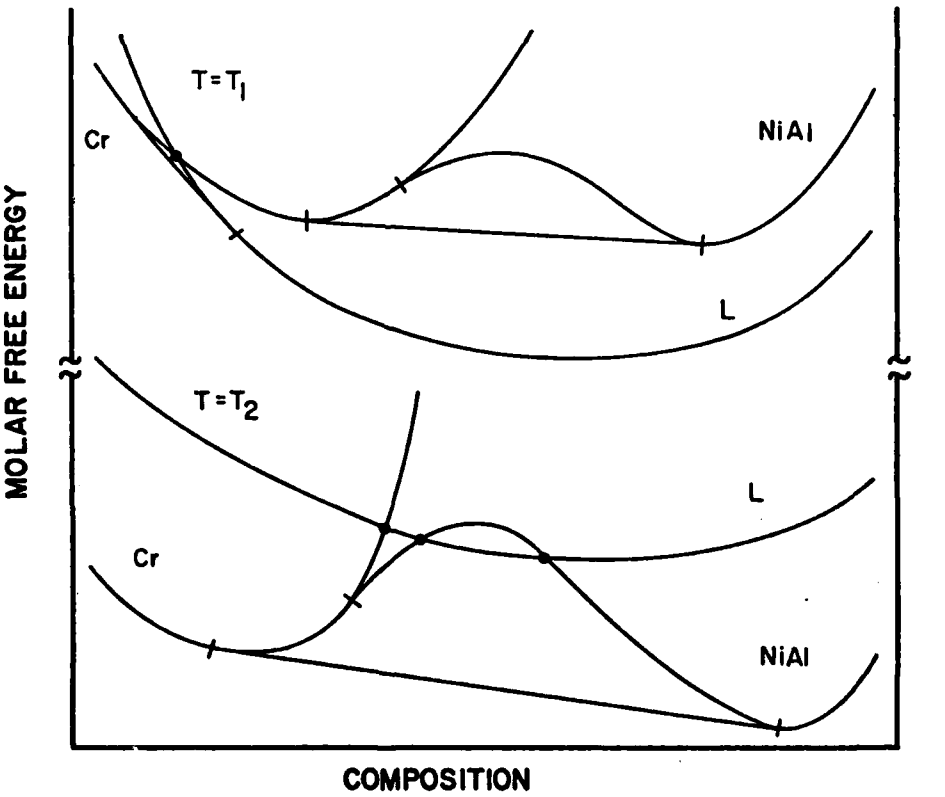
MOLAR FREE ENERGY
$T=T_1$
Cr
NiAl
L
$T=T_2$
L
Cr
NiAl
COMPOSITION

Fig 12

Published in Materials Science and Engineering, 65, 27-36 (1984).

MECHANISMS OF MICROSEGREGATION-FREE SOLIDIFICATION

W. J. Boettinger, S. R. Coriell

Metallurgy Division
National Bureau of Standards
Washington, DC 20234

and

R. F. Sekerka*

Carnegie-Mellon University
Pittsburgh, PA 15213

ABSTRACT

Two solidification mechanisms can produce microsegregation-free crystalline alloys: planar growth and partitionless solidification. For growth at high velocity, but still with equilibrium partitioning of solute, capillarity can stabilize a planar liquid-solid interface. This type of stability, known as absolute stability, has been confirmed experimentally for Ag-Cu alloys and should apply only when the net heat flow is towards the solid. Another possibility for producing microsegregation-free alloys is partitionless solidification which can occur at high velocities and arises from the kinetics of interface motion. These kinetics involve the trapping of solute by the moving interface, causing the partition coefficient to be unity. A unified model for the variation of the interface temperature and partition coefficient with interface velocity is presented. This model spans the range from slow velocities, where local equilibrium is usually valid, to high velocities where partitionless solidification occurs. Considerations necessary to predict the conditions of microsegregation-free solidification for concentrated alloys are also discussed.

*Consultant, Metallurgy Division, National Bureau of Standards

Introduction

Microsegregation-free crystalline alloys, including those with solute in excess of equilibrium solubility, provide an ideal starting microstructure for the development of interesting mechanical properties during subsequent thermomechanical processing [1]. In this paper, three topics related to the solidification conditions required to produce such microstructures will be described: the interface temperature during solute trapping; the interface stability theory; and the conditions for microsegregation-free solidification of concentrated alloys. It will be assumed that the phase which is forming from the melt has been selected previously by nucleation kinetics or by competition among growing crystalline phases. Under this assumption, the primary role of nucleation is to allow the development of a large bulk undercooling of the liquid into which growth can occur quite rapidly. This paper focuses on the conditions at the solid-liquid interface, with the realization that a full analysis of heat and solute transport must be conducted to form the basis for a final choice of processing conditions.

Interface Conditions

In 1971, Baker and Cahn [2] posed the interface conditions for solidification of a binary alloy by using two response functions. One choice for the response functions describes the interface temperature, T_I, and the composition of the solid at the interface, C_s^*. These response functions can be written as follows:

$$T_I = f(V,C_L^*) - T_M\Gamma K \qquad (1)$$

$$C_S^* = C_L^* k(V,C_L^*) \qquad (2)$$

where V is the local interface velocity, C_L^* is the composition of the liquid at the interface, $T_M\Gamma$ is a capillarity constant, and K is the mean curvature of the solid-liquid interface. The explicit dependence of k on curvature is neglected. At zero velocity, the functions f and k are very simply related to the phase diagram: $f(0,C_L^*)$ is the equation for the phase diagram liquidus and $k(0,C_L^*)$ is the equation for the equilibrium partition coefficient, k_E, which can depend on composition.

These response functions are constrained by thermodynamics. Fig. 1 shows the molar free energy versus composition for a liquid and a solid phase at a fixed temperature. During solidification, the temperature and the compositions at the interface are constrained by the fact that there must be a net decrease in the free energy per mole, ΔG, needed to form an infinitesimal amount of solid of composition C_S^* from liquid of composition C_L^* [2]. The free energy change is shown in Fig. 1, and is given by

$$\Delta G = (\mu_S^A - \mu_L^A)(1-C_S^*) + (\mu_S^B - \mu_L^B)C_S^*. \qquad (3)$$

Under the usual assumption of local equilibrium at the solid-liquid interface, believed to be valid at slow rates of solidification, the chemical potentials of the liquid, μ_L^i, and solid, μ_S^i, for each species, i, must be equal.

During rapid rates of solidification, this is not necessarily the case and nonequilibrium conditions at the interface can exist. The term solute trapping is loosely applied to conditions when the partition coefficient deviates from the equilibrium value, but as originally defined, is restricted to the case when the chemical potential of the solute increases during solidification. Baker and Cahn showed that the restriction that ΔG be negative could be represented on a figure where, for constant temperature, the range of possible solid and liquid concentrations at the interface are shown. Fig. 2 shows an alternate representation of this restriction [3]. The cross-hatched region shows the range of possible solid compositions that can form from a liquid of composition C_L^* at various temperatures. When the temperature is equal to the liquidus temperature for the composition C_L^*, the only possible solid composition is the equilibrium solid composition. For interface temperatures below the liquidus, the range of allowable solid composition expands. Of particular interest is the T_0 curve which lies between the liquidus and the solidus. The T_0 curve is the locus of compositions and temperatures for which the molar free energy of the liquid and solid phases are equal. When the temperature of the liquid at the interface reaches the T_0 curve, the solid can have the same composition as the liquid, i.e., partitionless solidification. Fig. 2b shows a case where the T_0 curve plunges quite steeply. In this case, for the composition C_L^*, partitionless solidification is not possible, i.e., the partition coefficient, k, cannot approach unity at high velocity. The impossibility of partitionless solidification has been associated with glass formation [3].

Several models for the dependence of the partition coefficient on velocity have been formulated [4-7]. This dependence on velocity constitutes one of the two response functions required to analyze rapid solidification

problems. The model formulated by Baker [4] is quite general and includes a wide variety of possibilities. Fig. 3 shows the results of more recent theories which predict that the partition coefficient changes monotonically from its equilibrium value to unity as the growth velocity increases. In these models the interface partition coefficient is a function of a dimensionless velocity, $\beta_0 V$, where β_0 is the ratio of a length scale, a_0, normally related to the interatomic distance and a diffusion coefficient, D. The diffusion coefficient in the various models ranges between a liquid diffusion coefficient and a diffusion coefficient characteristic of the interface itself. The functional form of the model proposed by Aziz [5] and Jackson, Gilmer and Leamy [6] for continuous growth is given as

$$k(V) = \frac{k_E + \beta_0 V}{1 + \beta_0 V} \tag{4}$$

where $\beta_0 = a_0/D$. At a velocity of $1/\beta_0$, the partition coefficient is the average of the equilibrium partition coefficient and unity. If we choose a liquid diffusion coefficient typical of metals (10^{-5} cm^2/s) and the length scale to be 5A, $1/\beta_0$ is 200 cm/s. However, the value of $1/\beta_0$ which best fits [5] recent experimental data for doped Si is 10 m/s; for Si, $D = 5 \times 10^{-4}$ cm^2/s [8], and hence a_0 = 50 A. It remains a challenge to design good experiments to determine the velocity required for solute trapping in metallic alloys.

There are significant shortcomings in the present models of the dependence of the partition coefficient on velocity. The models primarily treat dilute alloys so there is no explicit dependence on composition. For the case of Fig. 2b, where the T_0 curve plunges, the partition coefficient cannot approach unity at high velocity. A second shortcoming of the present trapping models is that the response function for the interface temperature is not treated.

Following the suggestion of Aziz [5] a response function for the interface temperature, consistent with a velocity dependent partition coefficient, can be formulated. For pure materials Turnbull et al. [9,10] have suggested that the rate at which atoms attach to the growing crystalline solid may only be limited by their rate of collision with the solid. In such a case, the interface velocity is related to the interface temperature, T_I, by an expression

$$V = fV_0\{1-\exp(\Delta G/RT_I)\} \tag{5}$$

where f is the fraction of sites on the solid-liquid interface available for attachment, V_0 is the speed of sound in the liquid metal, ΔG is the molar free energy for solidification and R is the gas constant. For most metals, f is thought to be close to unity and for velocities much less than the speed of sound, this expression can be written as

$$V = -V_0\left(\frac{\Delta G}{RT_I}\right) \tag{6}$$

For the solidification of disordered crystals, this collision limited model of solidification may apply as well. The molar free energy for solidification of alloys is evaluated from Eq. (3) and, in special cases, can be described simply in terms of undercooling. When solute trapping occurs a simple expression in terms of undercooling is not possible. For the special case of a pure material ΔG reduces to

$$\Delta G = \frac{-L(T_M - T_I)}{T_M} \tag{7}$$

where L is a latent heat and T_M is the melting point of the pure metal. For dilute alloys, when the partition coefficient equals the equilibrium partition coefficient, k_E, the thermodynamic driving force for solidification is given by

$$\Delta G = \frac{-L(T_L - T_I)}{T_L} \tag{8}$$

where T_L is the liquidus temperature for the concentration of the liquid at the interface C_L^*. When the partition coefficient is identically equal to one, ΔG has a similar form,

$$\Delta G = \frac{-L\ (T_o - T_I)}{T_o} \tag{9}$$

where the undercooling $(T_o - T_I)$ is referred to the T_o temperature for the interface composition. The similarity of the expressions for the case

where k equals one, i.e., partitionless solidification, and the expression for pure metals, is the origin of the often stated idea that the kinetics of partitionless solidification are quite rapid and similar to that for the solidification of a pure metal. In the general case when the partition coefficient is not the equilibrium value, the thermodynamic driving force for solidification must be evaluated from the full expression given by Eq. (3). In this expression the chemical potentials are functions of concentration and temperature that may be determined by modelling the phase diagram. This demonstrates the importance of modelling phase diagrams, even for applications to rapid solidification. If Eqs. (3 & 5) are combined with, for example, the trapping model of Aziz, Eq. (4), the interface temperature and the solid composition at the interface can be determined as functions of the interface velocity and the concentration of the liquid at the interface. A similar calculation for other models of solute trapping or interface temperature can be performed. Alternatively, part of the free energy for solidification can be dissipated by solute drag [11].

Fig. 4 shows a composite plot of the two response functions obtained by using Eqs. (3-5) superimposed on the phase diagram including the liquidus, solidus and T_0 curve. The composition of the solid at the interface and the interface temperature are plotted along a curve parameterized by interface velocity for a given fixed liquid concentration at the interface. The figure is based on thermodynamic data for Ag-Cu [12], a liquid composition at the interface of 8.2 at% Cu, a value of β_0 of 10^{-2} s/cm and for two values of V_0 (infinity and 2×10^5 cm/s). At zero velocity, the composition of the solid lies on the solidus curve. At intermediate velocities (~10 cm/s),

the concentration of the solid moves towards the concentration of the liquid with a small increase in the undercooling. At high velocities the solid composition at the interface approaches the liquid concentration at the interface near the T_0 curve. The dashed curve shows the case where V_0 is infinite. This curve corresponds to the thermodynamic bound on the solid concentration at the interface given in the Fig. 2. The dashed curve can also be obtained by letting $\Delta G = 0$ in Eq. (3). The solid curve, for a finite value of V_0, shows the interface temperature plunging quite rapidly. This analysis provides, for the first time, a pair of thermodynamically consistent response functions for the conditions at the liquid-solid interface. When combined with solute redistribution and heat flow analysis, these functions permit the analysis of rapid solidification problems. For example, a more precise analysis of recalescense [13-16] is possible. During recalescence, the velocity of the interface decreases due to the evolution of latent heat. They are also required for a detailed analysis of the stability of the solid-liquid interface during solute trapping.

Interface Stability

Interface stability theory is of interest because, during planar growth, solidification occurs with no lateral microsegregation. The theory was first developed by Mullins and Sekerka [17] and has been extended and discussed in more detail for rapid solidification by Coriell and Sekerka [18-19]. Others have applied this theory to various rapid solidification results [3, 8, 20, 21]. The present paper is restricted to a discussion of the simple asymptotic form of the stability theory relevant at high velocity. This asymptotic form is known as absolute stability and is given by the expression

$$V = \frac{mD(1 - k_E)C}{k_E^2 T_M \Gamma} \tag{10}$$

where m is the liquidus slope, D is the liquid diffusion coefficient and C is the alloy composition. Whenever V exceeds the value given in Eq. (10), a planar liquid-solid interface is stable. Absolute stability of a planar interface occurs because of the influence of capillarity. At high growth velocities, there is only limited time available so lateral solute segregation in the liquid can only occur for perturbations of the solid-liquid interface with very short wavelengths. These short wavelengths require such a large increase in the area of the interface that the perturbations are retarded by capillary forces and the interface is stable.

There are several restrictions on the use of the simple asymptotic form given by Eq. (10). First, rather trivially, this form is only valid if the partition coefficient is the equilibrium partition coefficient. Modifications required when the partition coefficient depends on the velocity will be discussed in a later section. A second restriction is that the net heat flow must be into the solid, i.e.,

$$G^* = \frac{k_L G_L + k_S G_S}{k_L + k_S} > 0 \tag{11}$$

Here k_L and k_S are the thermal conductivities of the liquid and solid respectively. G_L and G_S are the temperature gradients in the liquid and

solid respectively. In the case of solidification following surface melting, the conduction of heat is almost completely into the solid and G^* is always positive. For quenching against a substrate or for atomization, the sign of G^* is less clear. What is important is the relative amount of heat flowing into the solid compared to that flowing into the liquid. For quenching against a substrate, bulk undercooling of the liquid can occur if nucleation is difficult. In this case, during solidification heat can flow both into the solid and into the liquid to remove the latent heat evolved at the liquid-solid interface. An experimental observation in which planar growth is stable, and G^* is negative, would require a reexamination of the assumptions in the present stability theory. In this event two possible modifications [18] would be an allowance for a velocity of solidification that depends on time or an analysis of solidification in samples in which the wavelength of the fastest growing instability is of the same order as the sample itself. A third restriction on the use of the absolute stability equation is that one must be far from the modified constitutional supercooling regime of the full stability theory. This condition will be satisfied whenever the velocity

$$V >> \frac{LD^2}{(k_s + k_L)T_M\Gamma k_E} \tag{12}$$

provided also that the temperature gradient in the liquid is not too large [$G_L << VL/(2k_L)$] as is usually the case for rapid solidification. Here, L is the latent heat per unit volume. This restriction is more important for doped Si [19] than for metallic alloys due to the relatively high latent heat and diffusion coefficient for Si.

In a recent set of experiments employing electron beam surface melting [22] the applicability of the morphological stability theory to rapid solidification has been demonstrated. Fig. (5) shows the transition from cellular to cell-free structure which occurs in Ag-1 wt% Cu and Ag-5 wt% Cu alloys. For the former, the transition occurs between 10 and 20 cm/s, and for the latter, the transition occurs between 50 and 60 cm/s. Fig. 6 shows a summary of the experimental results for the two alloys. The transition from cellular to cell-free material is seen to occur at velocities roughly a factor of 2 less than the theoretical predictions. Such agreement is considered reasonable in view of the imprecise knowledge of the materials parameters required for the theory.

When the partition coefficient depends on the interface velocity, the stability theory must be modified [23]. This modified analysis of stability suggests the possibilty of increased instability of a planar liquid-solid interface, attributed to a feature called the "solute pump mechanism". Physically, the partition coefficient will vary across a perturbed solid-liquid interface because of local differences in velocity. This leads to a variation of the solute rejection rate along the interface and produces lateral solute segregation without the necessity of lateral diffusion. Hence perturbations with wavelengths much longer than those normally encountered at high growth velocity can occur and capillarity is less effective in stabilizing such perturbations. The results of the theory are complex and will only be described qualitatively here. It is found that the actual value of the partition coefficient can be substituted into the absolute stability equation only under certain conditions. If the rate of change of the partition coefficient with velocity is relatively small, and/or the absolute value of the rate of change of the interface temperature

with respect to velocity is relatively large, this simple substitution method is valid. On the other hand, if the rate of change of the partition coefficient with velocity is large and/or the absolute value of the rate of change of the interface temperature with velocity is small, the simple substitution is not valid. Clearly the details of the size of these derivatives depends critically on the parameters β_0 and V_0 described in the previous section. Fig. 7 shows a plot of the demarcation between stability and instability for Ag-Cu alloys for a choice of β_0 of 10^{-2} s/cm and for various values of μ_T where $\mu_T = - \partial V/\partial T_I$. On the right side of the figure is shown the variation of the partition coefficient with velocity. On the left side is shown the demarcation between stability and instability. Depending upon the value of μ_T, the stability criterion can change dramatically.

It should be pointed out that the instability in the case of the "solute pump mechanism" is oscillatory in nature. This arises because of the temporal phase difference between the local velocity of the interface and the interface shape. Such oscillatory instabilities lead to microsegregation patterns that are three dimensional, whereas an ordinary microsegregation pattern is two dimensional (in directions transverse to the growth direction). Such oscillatory instabilities have not been observed, and only future experiments will determine their importance.

Concentrated Alloys

The solidification conditions required to produce microsegregation-free crystalline structures for concentrated alloys are generally associated with the temperature difference between the liquidus curve and the T_0 curve. For most terminal solid solutions, this difference increases with increasing concentration. The usual idea is that, compared to dilute alloys, such alloys require more rapid solidification or higher undercooling to produce microsegregation-free crystalline alloys. The simple trapping models presented earlier in this paper involve no explicit concentration dependence. Furthermore, a recent set of experiments conducted on Ag-rich Ag-Cu alloys [22], suggest that as the composition approaches the eutectic composition, the growth velocity required to form microsegregation-free structures decreases. At 15 wt% Cu, an interface velocity of approximately 2 m/s is required. At the eutectic composition (28 wt% Cu), a velocity of only 0.7 m/s is required. Therefore, in this alloy, it is actually easier to form the microsegregation-free structure for the very concentrated alloys. Such results have several possible origins and one possibility is related to the dependence of the liquid diffusion coefficient on temperature, as discussed below.

The dependence of the liquid diffusion coefficient on temperature is generally neglected in ordinary solidification theory. Such is the case because of the fact that solidification almost always takes place very close to the liquidus temperature. Diffusion data is often described by an Arrhenius equation. For a melting point of 1000K and an activation energy of 10 kcal/mol, an undercooling of 300K will reduce the diffusion coefficient by an order of magnitude.

The dependence of the diffusion coefficient on temperature can affect substantially various ideas in solidification. In the following, it is assumed that the diffusion coefficient is only a function of temperature. The first example involves solute redistribution in the growth of concentrated alloys. In particular it has been noted previously [3] that the dependence of the diffusion coefficient on temperature can lead to a maximum in eutectic growth rate of approximately 10 cm/s. This maximum velocity has origins that are identical with the nose of the C curve for eutectoid growth observed in solid state transformations. Such a maximum eutectic growth rate is consistent with the fact that eutectic spacings are rarely observed to be finer than 20 nm. A second example may occur in the stability theory. For planar growth with equilibrium at the solid-liquid interface, the interface temperature is at the solidus for the average alloy concentration. In many concentrated alloys, the solidus may easily lie 300 K below the liquidus. An order of magnitude change in the diffusion coefficient can affect the prediction of the stability theory significantly. A third example involves a very simple modification of the trapping model presented previously. The parameter β_0 involves a diffusion coefficient. A simple approach to include composition dependence in a trapping theory would be to calculate the diffusion coefficient at the T_0 temperature for various compositions. For pure silver, the diffusion coefficient is 2×10^{-5} cm^2/s at its melting point. For the eutectic composition the T_0 temperature is approximately 943 K and the diffusion coefficient, based on an activation energy of 10 kcal/mole, is 6×10^{-6} cm^2/s. This simple idea leads to the conclusion that the growth velocity required for significant

levels of solute trapping would be reduced by a factor of 3 as the composition changes from pure Ag to the eutectic composition. Such a trend is consistent with the observed data [22].

Conclusion

In this paper, a response function for the temperature of the interface during solute trapping has been discussed. This model for the temperature is consistent with thermodynamics and with models of solute trapping and collision limited growth. Such interface response functions should permit a rational approach to the solidification problem in a wide variety of conditions of heat flow and solute redistribution. Secondly, circumstances where the absolute stability equation can be used in lieu of the full stability theory have been addressed. Experimental results obtained by using electron beam surface melting of Ag-Cu alloys are consistent with the stability theory. Thirdly, a few comments have been presented on the conditions for microsegregation-free solidification of concentrated alloys. This area obviously remains ripe for experimental and theoretical investigation.

Acknowledgment

This work was partially sponsored by the Defense Advanced Research Projects Agency. One of us (RFS) received partial support from the National Science Foundation under grant DMR78-22462.

We would like to thank M. J. Aziz, J. W. Cahn, R. Mehrabian, R. J. Schaefer, and D. Turnbull for helpful discussions.

References

[1] M. Cohen and R. Mehrabian, Met. Trans. A, to be published.

[2] J. C. Baker and J. W. Cahn, in Solidification (ASM, Metals Park, 1971) p. 23.

[3] W. J. Boettinger, in Rapidly Solidified Amorphous and Crystalline Alloys, ed by B. H. Kear, B. C. Giessen and M. Cohen (Elsevier, 1982) p. 15.

[4] J. C. Baker, Interfacial Partitioning During Solidification, Ph.D. Thesis, MIT (1970) Chapter V. Also reported by J. W. Cahn, S. R. Coriell and W. J. Boettinger, in Laser and Electron Beam Processing of Materials, ed. by C. W. White and P. S. Peercy (Academic Press, NY, 1980) p. 89-103.

[5] M. J. Aziz, J. Appl. Phys. 53, 1158 (1982).

[6] K. A. Jackson, G. H. Gilmer, and H. J. Leamy, in: Laser and Electron Beam Processing of Materials, ed. by C. W. White and P. S. Peercy (Academic, NY, 1980) p. 104.

[7] R. F. Wood, Phys. Rev. B25, 2786 (1982).

[8] See, e.g., J. Narayan, J. Crystal Growth 59, 583 (1982).

[9] F. Spaepen and D. Turnbull, in Rapidly Quenched Metals, ed by N. J. Grant and B. C. Giessen (MIT Press, Cambridge, MA, 1976) p. 205.

[10] D. Turnbull and B. G. Bagley, in Treatise on Solid State Chemistry, ed. by N. B. Hannay (Plenum, New York, 1975) Vol. 5, p. 513.

[11] M. J. Aziz, Appl. Phys. Lett. to be published.

[12] J. L. Murray, Met. Trans. A, to be published.

[13] C. G. Levi and R. Mehrabian, Met. Trans. A, 13A, 221, 1982.

[14] J. H. Perepezko and I. E. Anderson, in "Synthesis and Properties of Metastable Phases," ed. by T. J. Rowland and E. S. Machlin, TMS-AIME, Warrendale, 31 (1980).

[15] Y. Shiohara, M. G. Chu, D. G. Macisaac, and M. C. Flemings, Rapidly Solidified Amorphous and Crystalline Alloys, ed. by B. H. Kear, B. C. Giessen, and M. Cohen (Elsevier, 1982) p 65.

[16] T. Z. Kattamis, Z. Metallkunde 61, 856, (1970).

[17] W. W. Mullins and R. F. Sekerka, J. Appl. Phys. 35, 444 (1964).

[18] S. R. Coriell and R. F. Sekerka, in Rapid Solidification Processing Principles and Technologies II, ed. by R. Mehrabian, B. H. Kear, and M. Cohen (Claitor, Baton Rouge, LA, 1980) p. 35.

[19] J. W. Cahn, S. R. Coriell, and W. J. Boettinger, in Laser and Electron Beam Processing of Materials, ed. by C. W. White and P. S. Peercy (Academic Press, New York, 1980) p. 89.

[20] R. J. Schaefer and R. Mehrabian, Mat. Res. Soc. Proc., 13, 733 (1983).

[21] S. P. Midson and H. Jones, in Rapidly Quenched Metals, ed. by T. Masumoto and K. Suzuki, The Japan Inst. of Metals, Sendai, (1982), 1539.

[22] W. J. Boettinger, R. J. Schaefer, F. S. Biancaniello, and D. Shechtman, Met. Trans. A, to be published.

[23] S. R. Coriell and R. F. Sekerka, J. Crystal Growth 61, 499 (1983).

FIGURE CAPTIONS

Fig. 1. Construction to show the Gibbs free energy per mole, ΔG, for solidification of an infinitesimal amount of solid of composition C_S^* from a liquid of composition C_L^* under nonequilibrium conditions for which the chemical potentials

$$\mu_L^A \neq \mu_S^A \text{ and } \mu_L^B \neq \mu_S^B.$$

Fig. 2. Regions (cross-hatched) of thermodynamically allowed solid compositions that may be formed when solid solidifies from liquid of composition C_L^* at various temperatures. The value of T_0 is the highest temperature at which partitionless solidification of a liquid of given composition can occur. In (b), the T_0 curve plunges and partitionless soldification is impossible for liquid of composition C_L^*. (From reference [3]).

Fig. 3. Curves showing the dependence of the interface partition coefficient, k, on velocity according to the models of various investigators.

Fig. 4. Interface temperature and solid compositions for solid that forms at the indicated velocities from a liquid of fixed composition C_L^* at the interface. Thermodynamic parameters are for Cu in Ag for a specific kinetic law with $V_0 = 2 \times 10^5$ cm/s (full curve) and $V_0 \to \infty$ (dashed curve).

Fig. 5. a) Cellular and b) cell-free structures obtained in Ag-1 wt% Cu alloys rapidly solidified at 10 and 20 cm/s respectively. c) Cellular and d) cell-free structures obtained in Ag-5 wt% Cu alloys rapidly solidified at 30 and 60 cm/s respectively TEM. (From reference [22].)

Fig. 6. Summary of structures obtained by electron beam surface melting and resolidification of Ag-1 and 5 wt% Cu alloys at various growth rates. The comparison of the absolute stability theory with experiments is shown.

Fig. 7. Curves showing the onset of morphological instability for nonequilibrium conditions for which the partition coefficient, k, varies with V as shown on the right. Velocity for instability is shown as a function of the composition of bulk liquid for various values of the kinetic coefficient μ_T. For $\mu_T \leq 1$, the transition to instability is non-oscillatory in time and corresponds to a simple substitution of k(V) into the standard criterion for instability. The units of μ_T are cm/(Ks).

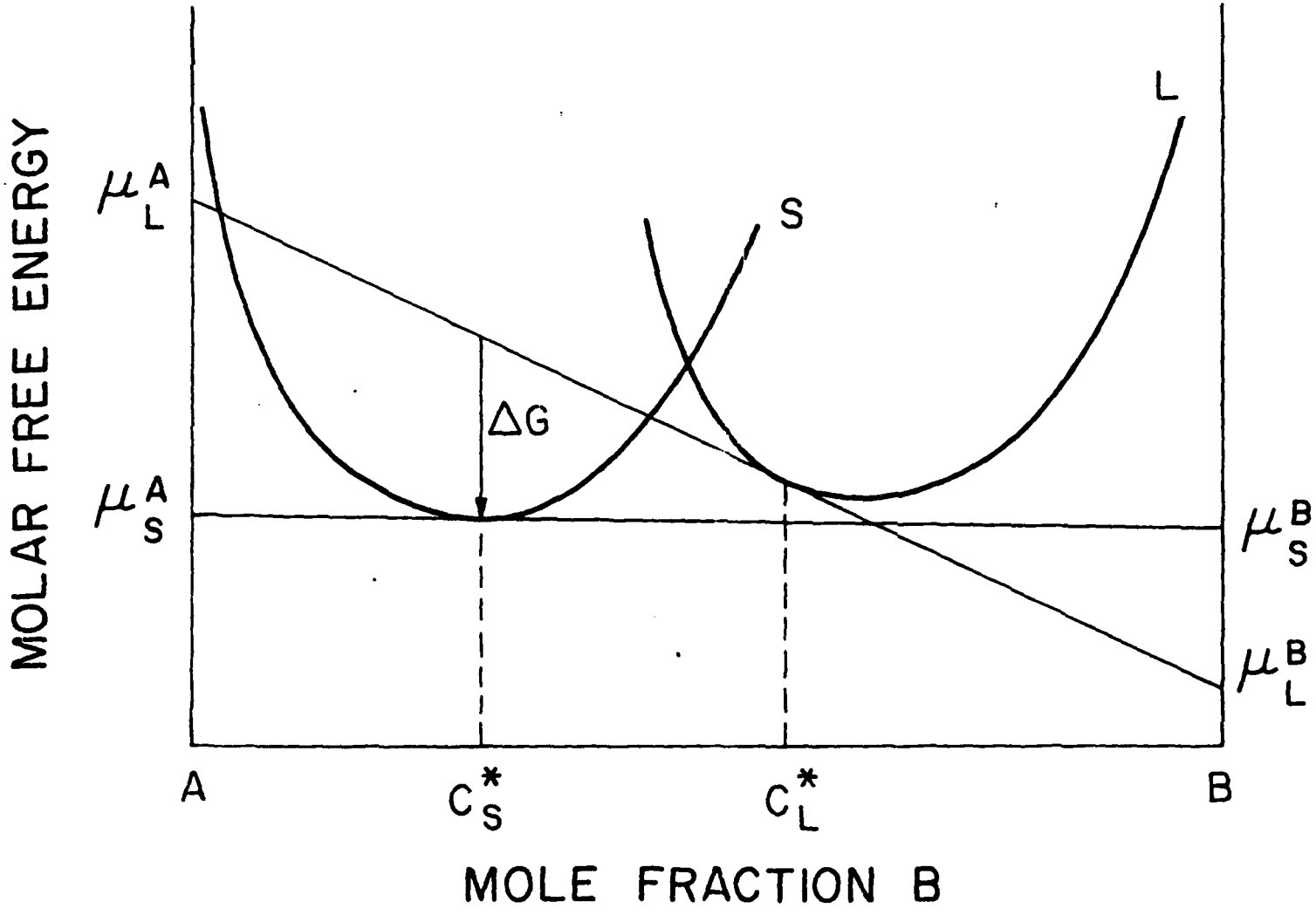
MOLAR FREE ENERGY
μ_L^A
μ_S^A
L
S
ΔG
μ_S^B
μ_L^B
A
C_S^*
C_L^*
B
MOLE FRACTION B

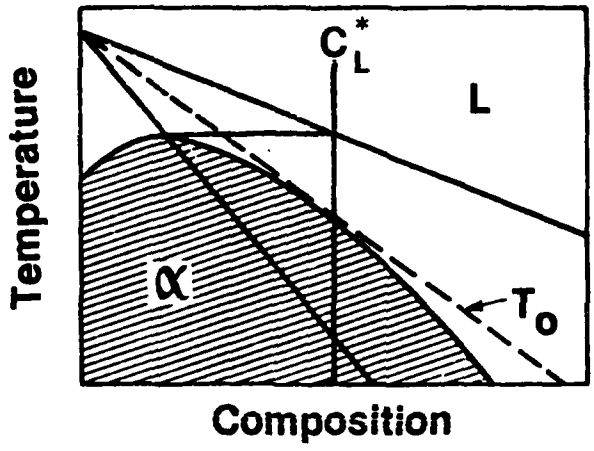
C_L^*
L
α
T_o
Temperature
Composition

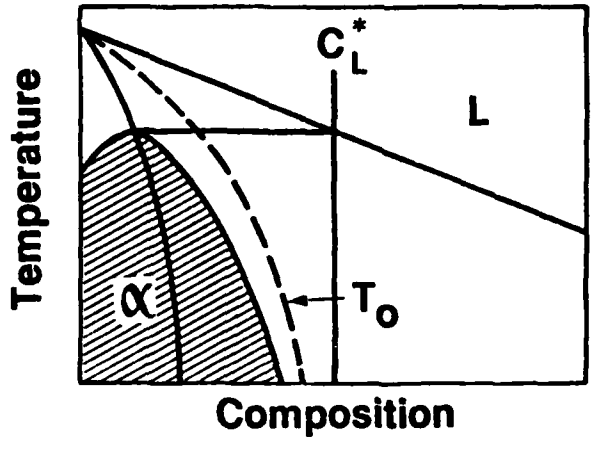
C_L^*
L
α
T_o
Temperature
Composition

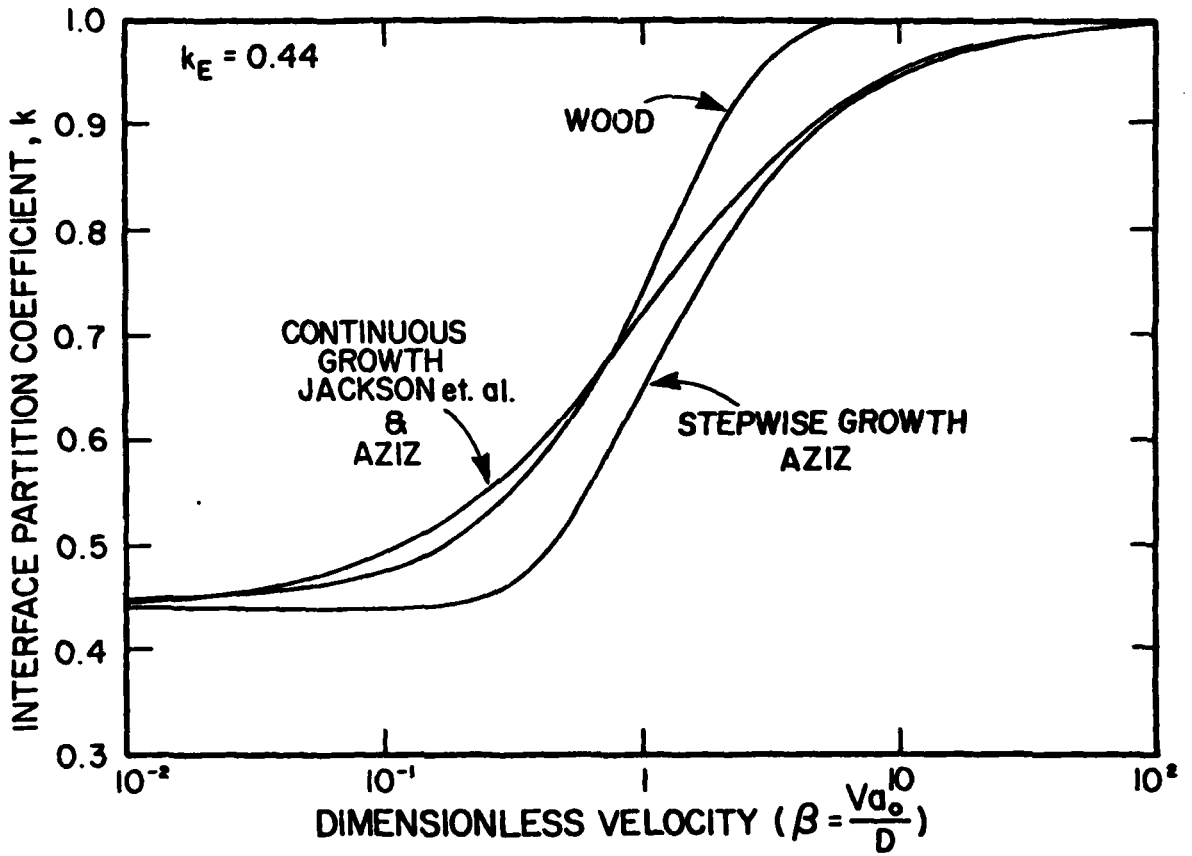
k_E = 0.44
WOOD
CONTINUOUS GROWTH JACKSON et. al. & AZIZ
STEPWISE GROWTH AZIZ
INTERFACE PARTITION COEFFICIENT, k
1.0
0.9
0.8
0.7
0.6
0.5
0.4
0.3
10^{-2}
10^{-1}
1
10
10^{2}
DIMENSIONLESS VELOCITY ($\beta = \frac{Va_o}{D}$)

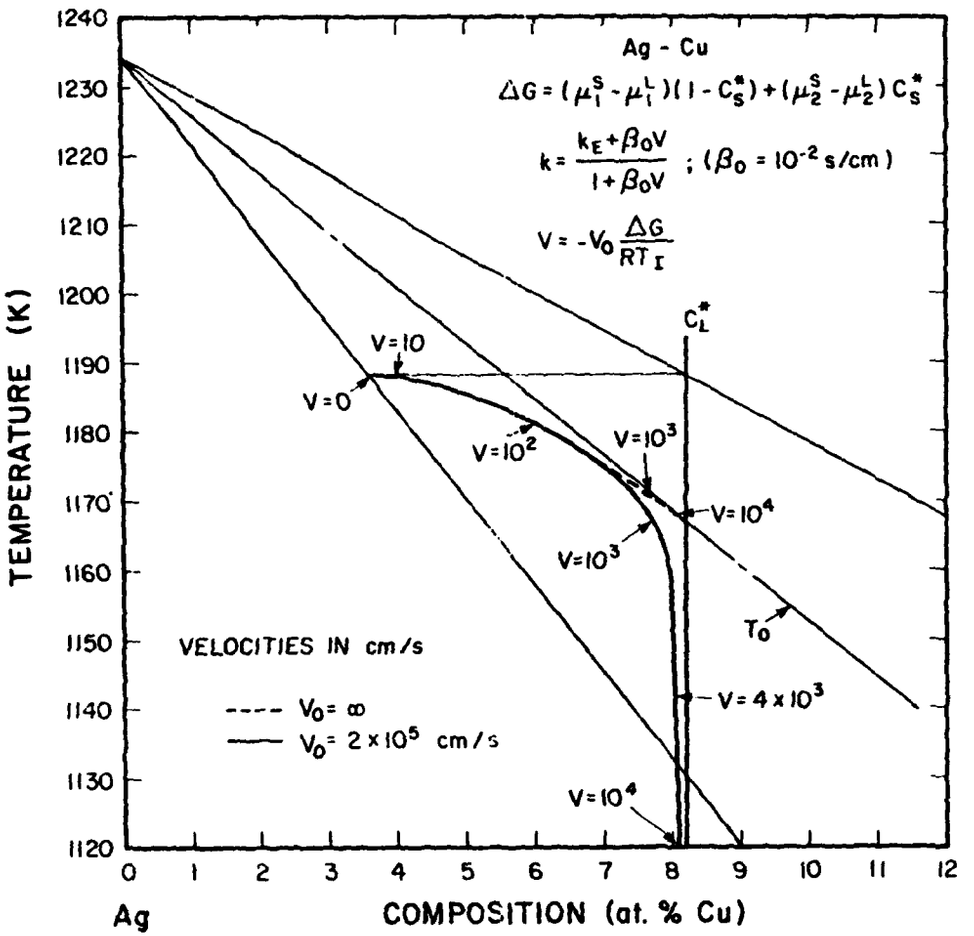
Ag - Cu
$\Delta G = (\mu_1^S - \mu_1^L)(1 - C_S^*) + (\mu_2^S - \mu_2^L) C_S^*$
$k = \frac{k_E + \beta_0 V}{1 + \beta_0 V}$; $(\beta_0 = 10^{-2}$ s/cm)
$V = -V_0 \frac{\Delta G}{RT_I}$
TEMPERATURE (K)
1240
1230
1220
1210
1200
1190
1180
1170
1160
1150
1140
1130
1120
C_L^*
V=10
V=0
$V=10^2$
$V=10^3$
$V=10^4$
$V=10^3$
T_0
$V = 4 \times 10^3$
$V=10^4$
VELOCITIES IN cm/s
---- $V_0 = \infty$
—— $V_0 = 2 \times 10^5$ cm/s
0 1 2 3 4 5 6 7 8 9 10 11 12
Ag
COMPOSITION (at. % Cu)

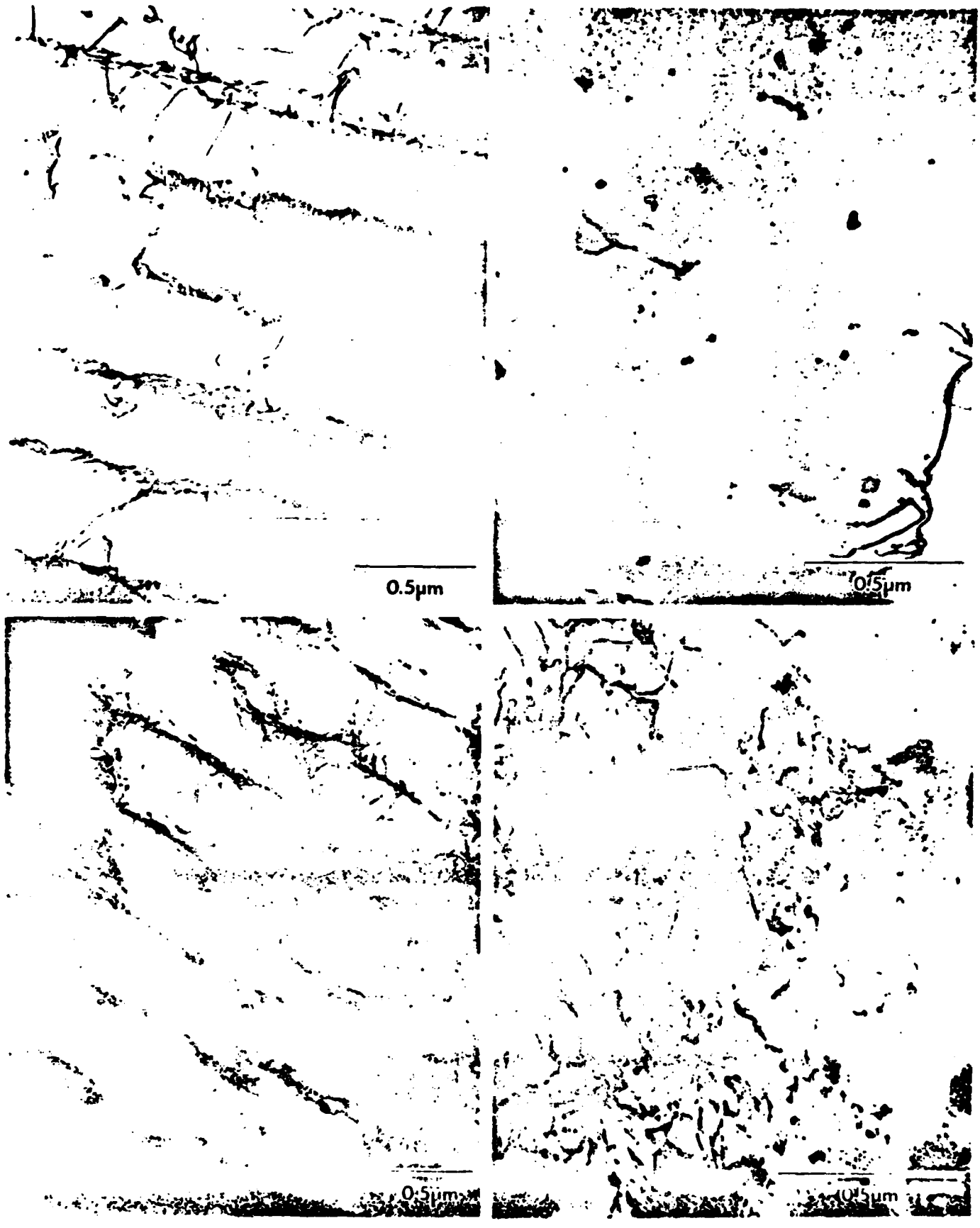
0.5μm
0.5μm
0.5μm
0.5μm

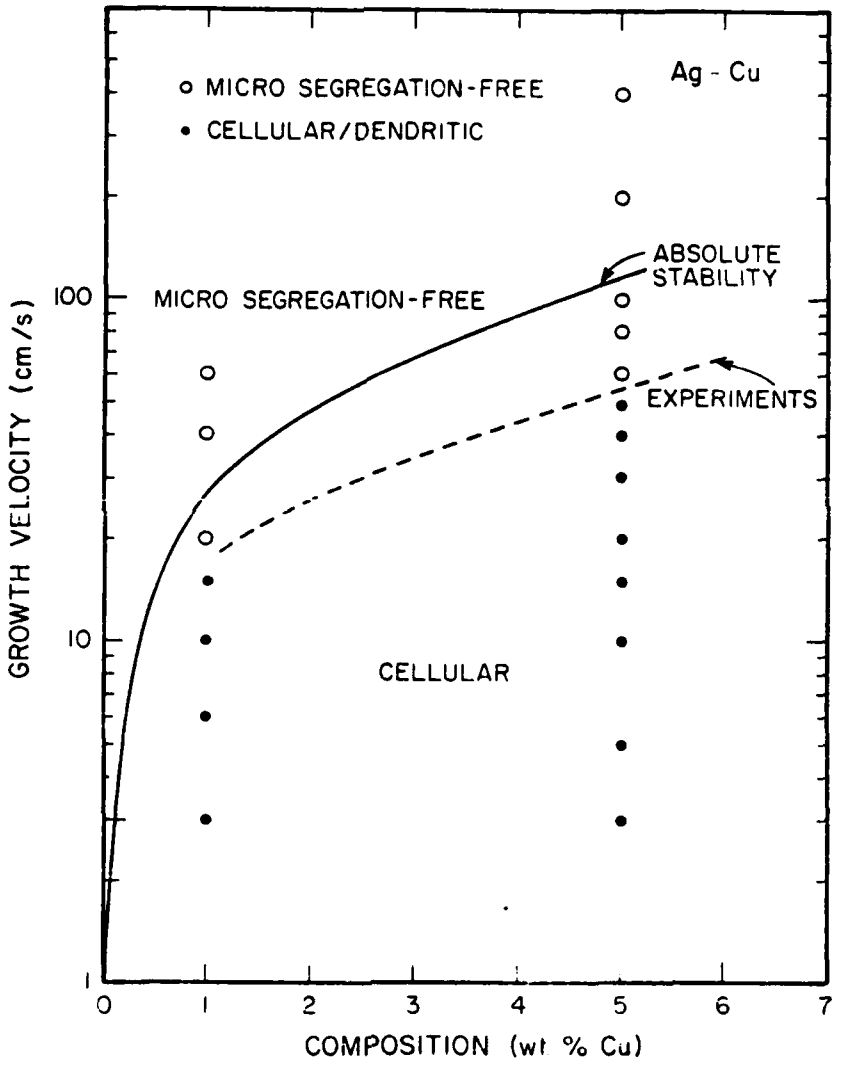
Ag - Cu
MICRO SEGREGATION-FREE
CELLULAR/DENDRITIC
ABSOLUTE STABILITY
MICRO SEGREGATION-FREE
EXPERIMENTS
CELLULAR
GROWTH VELOCITY (cm/s)
100
10
1
0
1
2
3
4
5
6
7
COMPOSITION (wt % Cu)

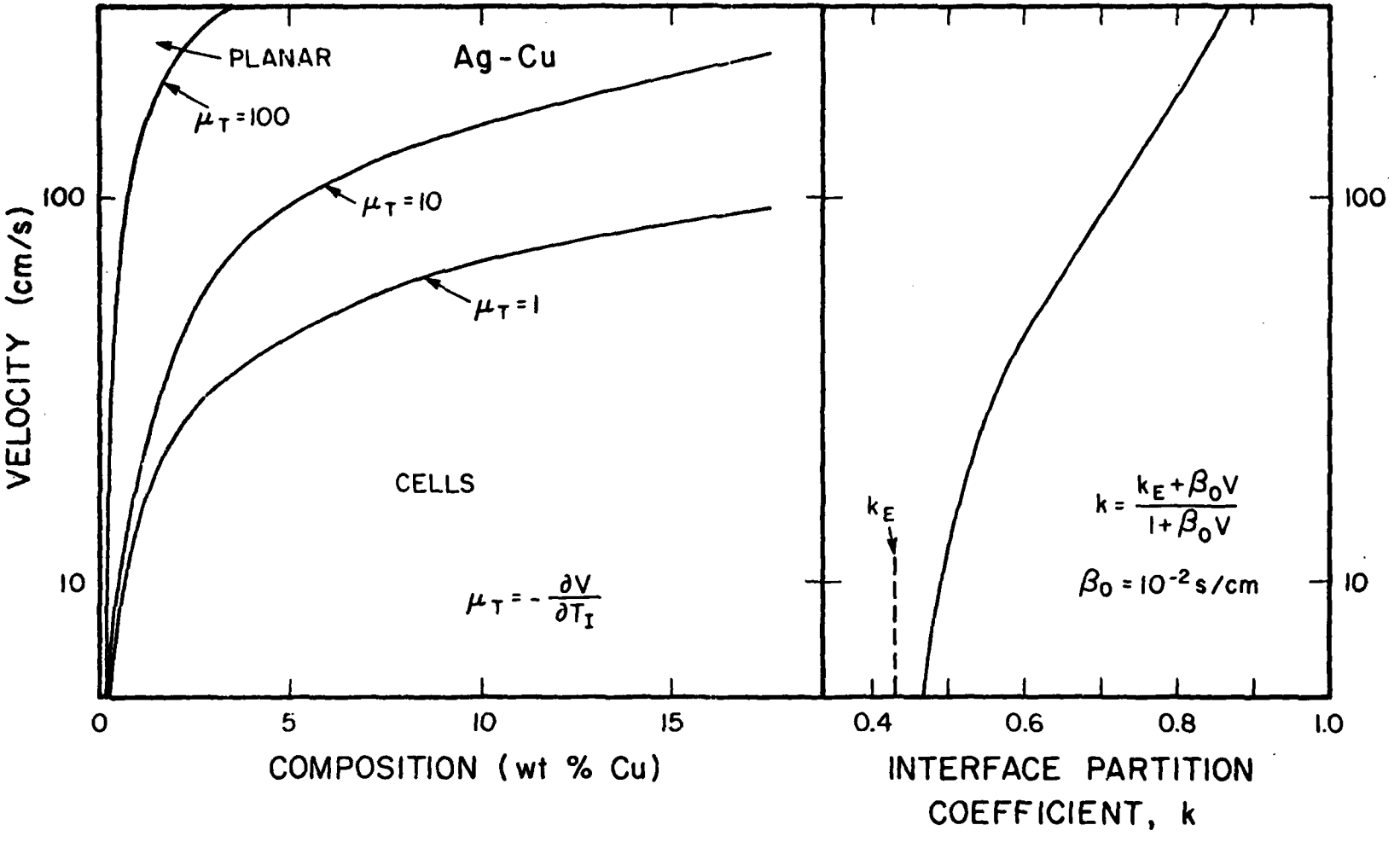
PLANAR
Ag - Cu
$\mu_T = 100$
$\mu_T = 10$
$\mu_T = 1$
CELLS
$\mu_T = -\frac{\partial V}{\partial T_I}$
VELOCITY (cm/s)
100
10
0
5
10
15
COMPOSITION (wt % Cu)
k_E
$k = \frac{k_E + \beta_0 V}{1 + \beta_0 V}$
$\beta_0 = 10^{-2}$ s/cm
0.4
0.6
0.8
1.0
INTERFACE PARTITION COEFFICIENT, k